

Article

The Late Triassic Molasse Deposits in Central Jilin Province, NE China: Constraints on the Paleo-Asian Ocean Closure

Zuozhen Han ^{1,2}, Jingjing Li ¹, Chenlin Zhu ¹, Wenjian Zhong ¹ and Zhigang Song ^{1,3,*} 

¹ Key Laboratory of Depositional Mineralization & Sedimentary Mineral of Shandong Province, College of Earth Science and Engineering, Shandong University of Science and Technology, Qingdao 266590, China; hanzuozhen@sdust.edu.cn (Z.H.); skdljj@sdust.edu.cn (J.L.); chenlinfongann@foxmail.com (C.Z.); zwjlangya@sdust.edu.cn (W.Z.)

² Laboratory for Marine Mineral Resources, Qingdao National Laboratory for Marine Science and Technology, Qingdao 266071, China

³ Research Center of Continental Dynamics, Shandong University of Science and Technology, Qingdao 266590, China

* Correspondence: zgsong@sdust.edu.cn

Abstract: This paper presents a new detailed study including zircon U-Pb-Hf isotopic, whole-rock geochemical and Sr-Nd isotopic analyses of conglomerate and granitic pebbles from the molasse deposits in central Jilin Province, NE China. These data are used to better constrain the Late Permian–Triassic tectonic evolution regarding particularly the final closure of the Paleo-Asian Ocean (PAO) along the Changchun–Yanji suture (CYS). Zircon U-Pb data indicate that the granitic pebbles formed in the end-Permian (254–253 Ma). The youngest detrital zircon age of 231 Ma from the conglomerate, and presence of the overlying Upper Triassic Sihetun Formation suggests that the molasse deposits on the Jin’gui Island formed during the Late Triassic. The end-Permian granitic rocks display high SiO₂ (66.07–74.77 wt %), with low MgO (0.55–2.05 wt %) and Mg# (31.61–43.64) values, together with depleted Hf and Nd isotopic values ($\epsilon_{\text{Hf}}(t) = +1.61$ to $+11.62$; $\epsilon_{\text{Nd}}(t) = +3.3$ to $+4.2$; $(^{87}\text{Sr}/^{86}\text{Sr})_i = 0.706458$ – 0.706842) and juvenile second-stage Hf model ages (1148–512 Ma), suggesting that they were probably generated by the partial melting of a Meso-Neoproterozoic juvenile metabasaltic lower crust. They are characterized by enrichments in large ion lithophile elements (LILEs) and depletions in high field strength elements (HFSEs), with affinities to igneous rocks forming in a subduction-related setting. This, combined with regional coeval subduction-related magmatic rocks, indicates that the PAO still existed along the CYS. In addition, the identification of Late Triassic molasse deposits on the Jin’gui Island in this study, coupled with occurrences of many Early Triassic syn-collisional granitoids along the CYS, indicates that the final closure of the PAO took place prior to the Late Triassic.

Keywords: molasse deposit; zircon U-Pb-Hf isotopes; geochemistry; NE China; Paleo-Asian Ocean



Citation: Han, Z.; Li, J.; Zhu, C.; Zhong, W.; Song, Z. The Late Triassic Molasse Deposits in Central Jilin Province, NE China: Constraints on the Paleo-Asian Ocean Closure. *Minerals* **2021**, *11*, 223. <https://doi.org/10.3390/min11020223>

Academic Editor: Clemente Recio

Received: 16 December 2020

Accepted: 19 February 2021

Published: 22 February 2021

Publisher’s Note: MDPI stays neutral with regard to jurisdictional claims in published maps and institutional affiliations.



Copyright: © 2021 by the authors. Licensee MDPI, Basel, Switzerland. This article is an open access article distributed under the terms and conditions of the Creative Commons Attribution (CC BY) license (<https://creativecommons.org/licenses/by/4.0/>).

1. Introduction

Northeast (NE) China, also called the Xing’an-Mongolian Orogenic Belt (XMOB), is located between the North China Craton (NCC) and Siberia Craton (SC) and is an important component of the Central Asian Orogenic Belt (CAOB; Figure 1a) [1–8]. It formed as a result of multiple subduction- and collision-related processes during the closure of the Paleo-Asian Ocean (PAO) and the amalgamation of micro-continental blocks with different origins and geological histories (Figure 1b) [4–15]. It is widely accepted that the Solonker-Xra Moron-Changchun-Yanji suture belt tectonically separates the NCC in the south from the micro-continental blocks in the north, and it marks the final closure of the Paleo-Asian Ocean [4–6,16–20]. Therefore, the timing of collision and formation of the Solonker-Xra Moron-Changchun-Yanji suture plays a significant role for us to understand the evolution of the PAO.

So far, although a large number of studies have investigated the sedimentology, paleobiogeography, magmatism, metamorphism, paleomagnetism, structural deformation, and tectonic evolution in the regions around the Changchun-Yanji suture (CYS) [21–53], some important aspects of the geology of this region, especially the precise time of the final closure of the PAO, still remain controversial. In one school of thought, the final closure occurred prior to the Permian, mainly including before the Late Devonian and between the Late Devonian [54–56] and Early Carboniferous [57–59]. In an alternative view, the closing of the PAO occurred during the Permian–Triassic, which can be reclassified as during the late Early Permian [60,61], during the Middle–Late Permian [62–65], during the Late Permian [4,34,48,66], during the Late Permian–Early Triassic [3,10,11,21,33,35,40,41,50,67–70], during the Late Permian–Middle Triassic [5,22,25,26,28,32,42,71,72], and during the Middle–Late Triassic [20,24,37,49,73]. Therefore, substantial controversy remains regarding the closure time of the PAO along the CYS.

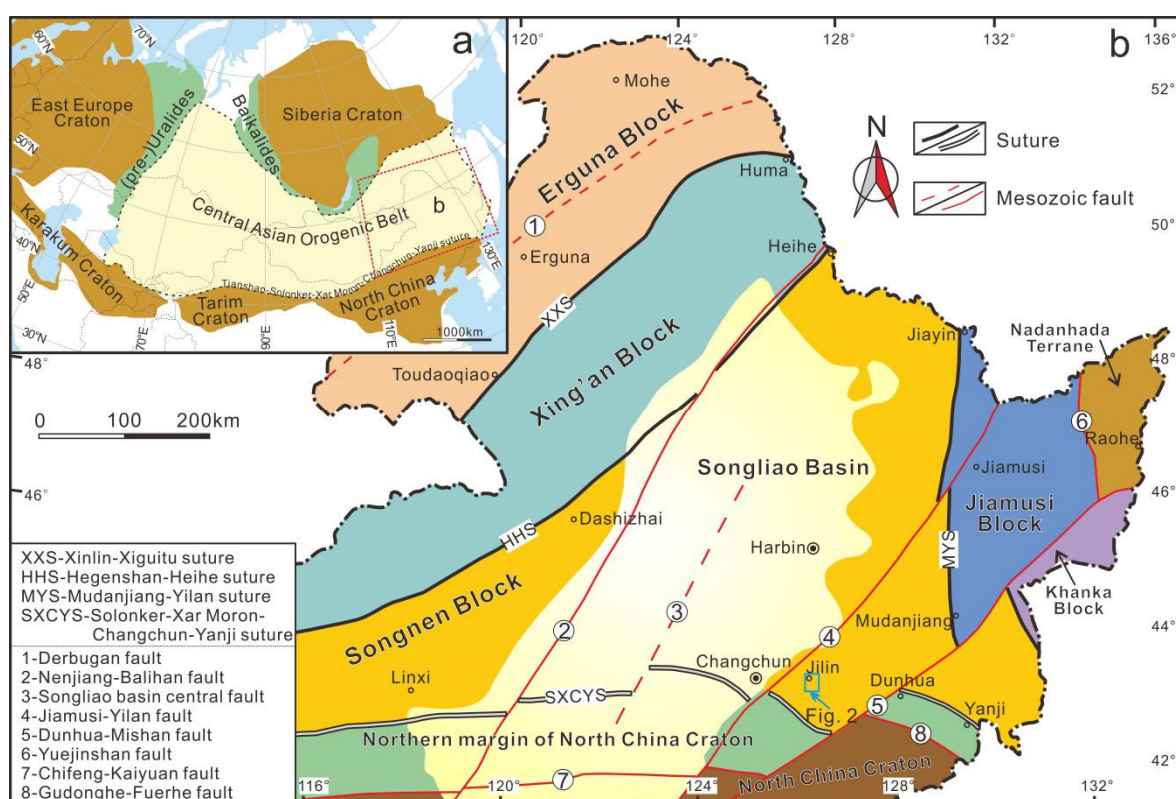


Figure 1. (a) Tectonic outline of the Central Asian Orogenic Belt (CAOB) and surrounding regions (modified from [74]); **(b)** Tectonic sketch map of NE China (modified from [5]).

Molasse generally provides ample evidence, present a record of regional tectonic evolutions, and have been widely applied to constrain the collision timing in the study of orogenic belt [46,75–77]. In this contribution, we focus on the Yangjiagou Formation in central Jilin Province, since this stratum tectonically experienced the evolution of the CYS and has the nature of molasse and carbonate deposits [78,79]. Here, we present novel zircon U-Pb dating, zircon Lu-Hf isotopic data, and whole-rock geochemical and Sr-Nd isotopic data for conglomerate and granitic pebbles within, from the molasse deposits of the Yangjiagou Formation in order to provide constraints on the Triassic tectonic evolution of the CYS and the timing of the final closure of the PAO.

2. Geological Setting and Sample Descriptions

2.1. Geological Setting

The central Jilin Province in NE China is located in the western part of the CYS at the junction of the Songnen Block and the NCC (Figure 1b). This region is adjacent to the Dunhua–Mishan Fault and the Songliao Basin to the east and west, respectively (Figure 1b). The CYS is composed mainly of Phanerozoic granitoids with a series of subduction-related tectonic mélanges, including the Kaiyuan, Xia’ertai, Hulan, Seluohe, Qinglongcun, and Kaishantun tectonic mélanges [12,15,21–23,25–28,31,35,47]. In addition, minor Paleozoic and Mesozoic sediments are also distributed in the “granite ocean” [39,43–46,48–50].

The study area is to the southeast of Jilin City, in central Jilin Province (Figure 2). According to the 1:200,000 geological map, this area mainly contains the Lower Permian Daheshen, the Upper Permian Fanjiatun and Yangjiagou, and the Triassic Xiaomifengdingzi formations [80] (Figure 2). The intrusive rocks include Triassic–Jurassic granitoids, in which the Jurassic monzogranite and granodiorite are the major components [80]. The Yangjiagou Formation is dominated by gray to greenish slate, siltstone, sandstone, conglomerate and tuffaceous breccia. This formation has a thickness of 500–1200 m and shows the nature of molasse formation.

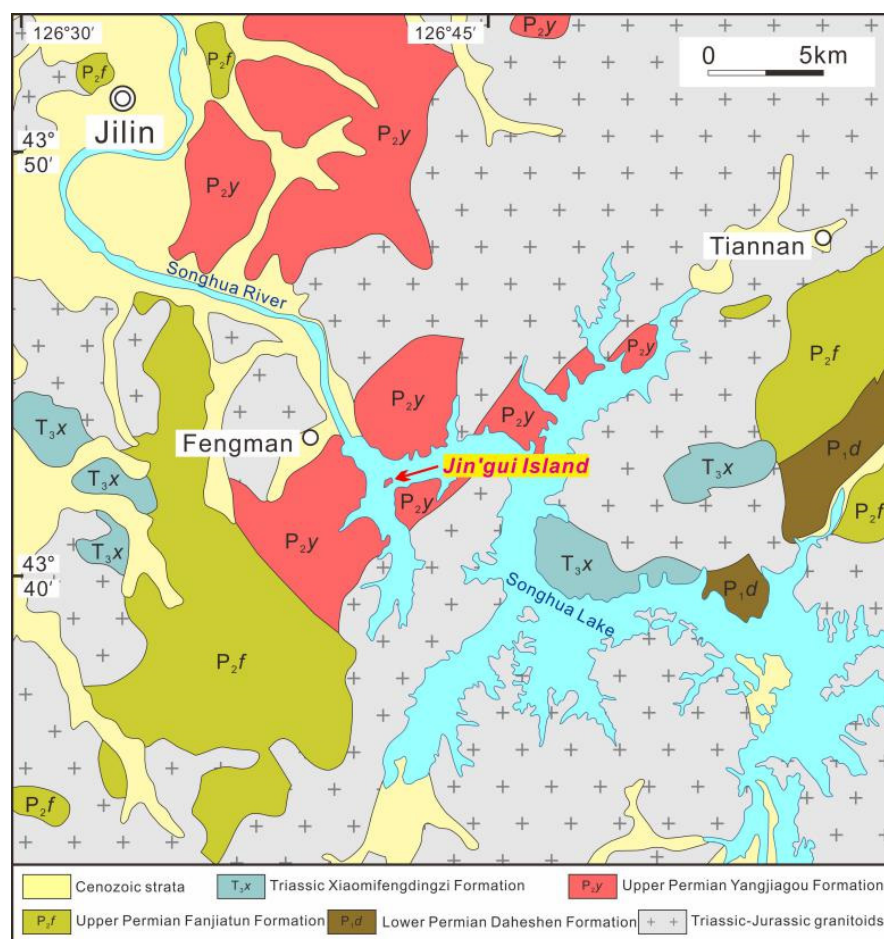


Figure 2. Geological map of the Songhua Lake area.

2.2. Sample Descriptions

The samples in this study were all collected from the Jin’gui Island in the Songhua Lake (Figure 2). Field observations suggest that pebble-bearing tectonic schist and conglomerate with complicated and high pebble content mainly crops out on the island. The rocks on this island were previously assigned to the Late Permian Yangjiagou Formation. The pebbles in the conglomerate are composed of granitic rocks, volcanic rocks (e.g., andesite), quartzite,

marble, and sandstone with poor sorting and roundness (Figure 3b–g). The lengths of pebbles generally range from 5 to 135 cm. Most pebbles are stretched and aligned in parallel to the fabric of the rock, which is indicative of plastic deformation and a strong strain effect on them.

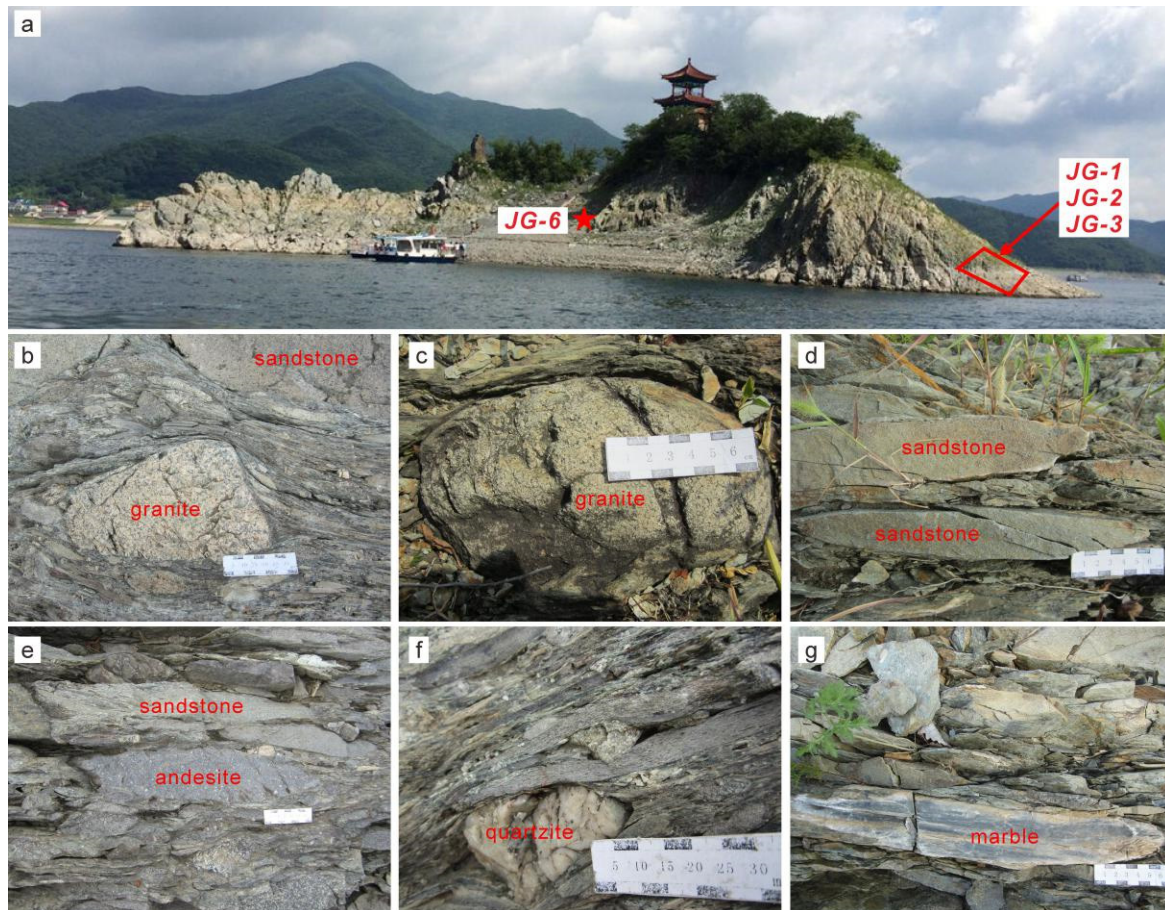


Figure 3. Field photographs of the Jin'gui Island showing (a) the sample locations and (b–g) different types of pebbles in the conglomerate.

To constrain the maximum depositional age of the sedimentary rocks on the Jin'gui Island, we collected one conglomerate sample (JG-6) and three granitic pebble samples (> 60 cm; JG-1, JG-2, and JG-3) whose locations are shown in Figure 3a.

The pebbles in the conglomerate sample (JG-6) are dominated by sandstone (90%) with minor granitic rocks (8%) and marble (2%). The matrix is grayish-green in color, crumbly, and shows well-developed foliations. It is composed mainly by quartz, plagioclase, biotite, sericite, chlorite, and opaque minerals (Figure 4a–c). Some of the quartz and feldspar grains exhibit brittle fracturing. Rotated quartz, feldspar and biotite porphyroclasts also can be observed.

Among the three granitic pebble samples, Sample JG-1 is a biotite monzogranite that consists mainly of plagioclase (40 vol %), alkali feldspar (30 vol %), quartz (25 vol %), and biotite (5 vol %) (Figure 4d). Sample JG-2 and Sample JG-3 are granodiorites that consists mainly of plagioclase (45–55 vol %), quartz (20–30 vol %), alkali feldspar (5–10 vol %), and hornblende (5 vol %) (Figure 4e,f). The granitic rocks also contain accessory zircon and Ti-Fe oxides.

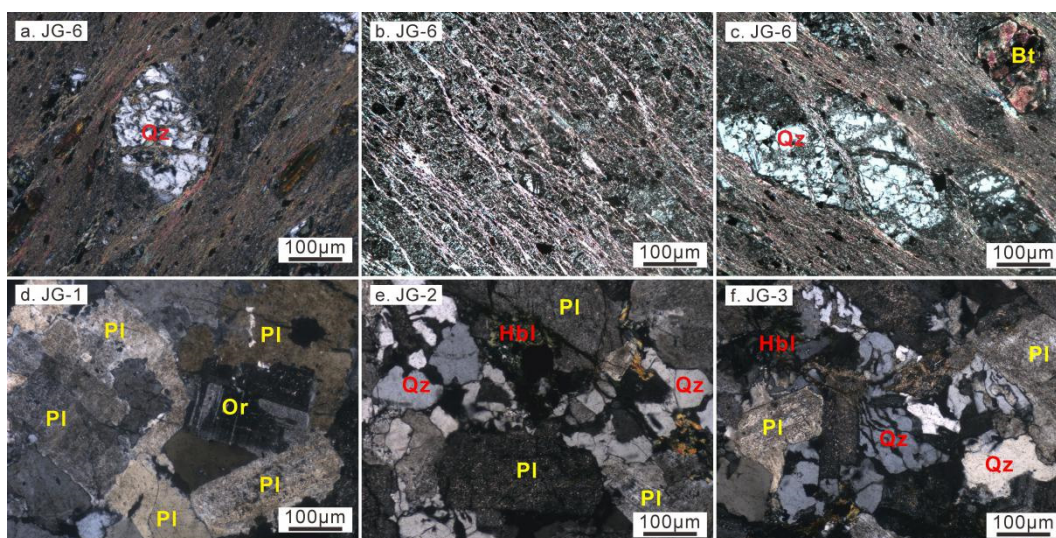


Figure 4. Photomicrographs of (a–c) matrix of the conglomerate and (d–f) granitic pebbles in the conglomerate. Mineral abbreviations according to [81]. plagioclase (Pl), quartz (Qz), biotite (Bt), hornblende (Hbl), orthoclase (Or).

3. Analytical Methods

The analytical techniques employed for zircon morphology, U–Pb geochronology, trace element compositions, in situ Lu–Hf isotopes, as well as whole-rock major and trace elements and Sr–Nd isotopes are presented in the Supplementary Materials.

4. Results

4.1. LA-ICP-MS Zircon Dating

Four samples including a conglomerate (JG-6) and three granitic pebbles (JG-1, JG-2, and JG-3) were selected for zircon U–Pb isotopic analyses. Representative cathodoluminescence (CL) images of analyzed zircons are shown in Figure 5. The analytical results are listed in Table S1. For statistical purposes, $^{207}\text{Pb}/^{206}\text{Pb}$ ages are used for grains >1000 Ma, whereas $^{206}\text{Pb}/^{238}\text{U}$ ages are used for grains <1000 Ma.

4.1.1. Conglomerate Sample JG-6

The majority of the zircons from this sample are euhedral to subhedral and exhibit a clear internal structure and fine-scale oscillatory growth zoning (Figure 5a), suggesting a low degree of reworking. However, a small number of zircons are rounded to subrounded and display blurry oscillatory or cloudy zoning (e.g., #81 and #183; Figure 5a), suggesting that they experienced multiple transportation events.

A total of 228 detrital zircon U–Pb ages were obtained, and all the ages are concordant (Figure 6a). The analyzed zircons range from 40 to 260 μm in size with length/width ratios of 1:1 to 3:1, and they contain Th and U contents of 8 to 793 ppm and 19 to 1519 ppm, respectively (Table S1). Generally, the Th/U ratio of metamorphic zircon is <0.1 and magmatic zircon is >0.4 [82–86], which can be used to distinguish the origin of zircons. A total of 228 detrital zircons were analyzed, most of which have Th/U ratios >0.4 , and there were 26 grains with ratios of 0.1–0.4 (predominately between 0.3 and 0.4; Table S1 and Figure 7a), indicating main magmatic origin. The concordant ages range between 2291 Ma and 231 Ma. Two grains generated $^{207}\text{Pb}/^{206}\text{Pb}$ ages of 2291 Ma and 1044 Ma, and one grain generated $^{206}\text{Pb}/^{238}\text{U}$ age of 802 Ma. Others have $^{206}\text{Pb}/^{238}\text{U}$ ages ranging from 529 to 231 Ma, and two primary peak ages are noted from the relative age probability diagram: (1) a remarkable peak value at 473 Ma in the range 529–426 Ma and (2) a remarkable peak value at 254 Ma in the range 334–231 Ma (Figure 6b).



Figure 5. Representative CL images of zircon from the (a) conglomerate and (b–d) granitic pebbles in the conglomerate. The solid-line and dash-line circles represent the locations for U–Pb dating and in situ Lu–Hf isotope analysis, respectively. The numbers show the ages of the zircons (Ma) and the $\epsilon_{\text{Hf}}(t)$ values.

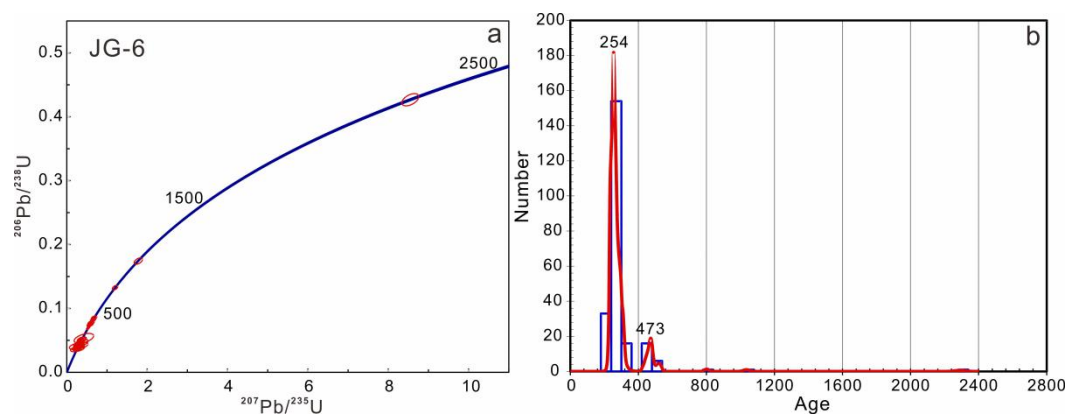


Figure 6. (a) U–Pb concordia and (b) probability diagrams of zircon ages for the conglomerate sample JG-6.

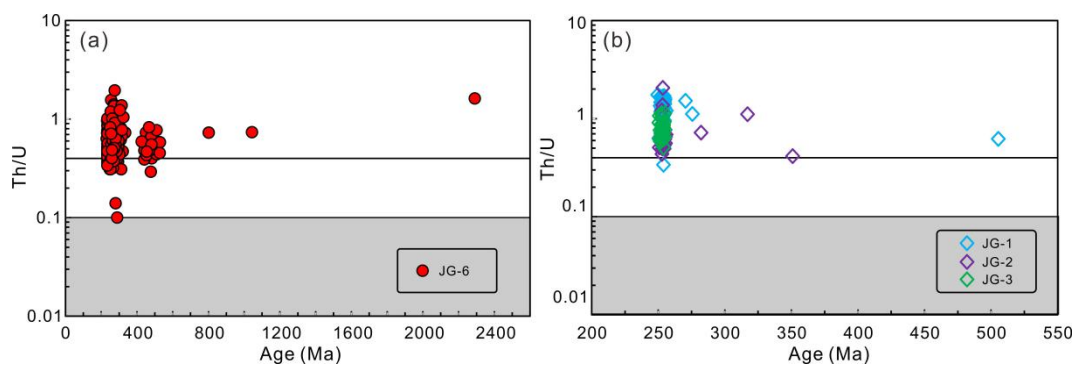


Figure 7. Th/U ratio vs. U–Pb ages diagram for zircons from the (a) conglomerate and (b) granitic pebbles in the conglomerate. The shaded area denotes values for typical metamorphic zircons with Th/U < 0.1.

4.1.2. Granitic Pebble Samples

Zircons from the three granitic pebble samples are generally ally euhedral–subhedral in shape and have the length ranging from 50 to 260 μm , while the length-to-width ratios are from 1:1 to 2:1. CL imaging revealed that these zircons show clear fine-scale oscillatory growth zoning, showing the features of magmatic zircons (Figure 5b–d), which are further supported by their high Th/U ratios (0.34–2.06, average 0.92; Table S1 and Figure 7b).

Sample JG-1 (Biotite Monzogranite)

Forty-two analyses were made on 42 zircons from sample JG-1, and 39 concordant ages were obtained (Table S1). With the exception of three spots that yielded ages of 506 ± 10 Ma, 276 ± 7 Ma, and 270 ± 4 Ma, a total of 36 analyses yielded a weighted mean $^{206}\text{Pb}/^{238}\text{U}$ age of 254 ± 2 Ma (MSWD = 0.065, $n = 36$; Figure 8a), representing the emplacement age of the biotite monzogranite; the three older ages represent the ages of inherited or captured zircons entrained by the granitic magma.

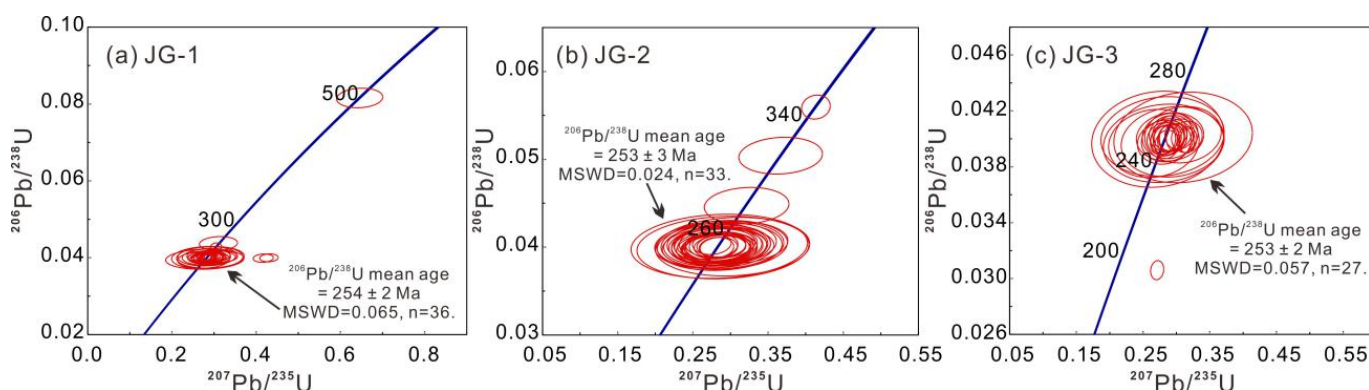


Figure 8. U–Pb concordia diagrams of zircon ages for the granitic pebbles in the conglomerate. (a) sample JG-1; (b) sample JG-2; (c) sample JG-3.

Sample JG-2 (Granodiorite)

Thirty-six zircon grains from sample JG-2 were analyzed, and 33 of them gave $^{206}\text{Pb}/^{238}\text{U}$ ages ranging from 256 to 251 Ma, yielding a weighted mean $^{206}\text{Pb}/^{238}\text{U}$ age of 253 ± 3 Ma (MSWD = 0.024, $n = 33$; Figure 8b), which is interpreted as the emplacement age of the granodiorite. The other three spots gave $^{206}\text{Pb}/^{238}\text{U}$ age of 351 ± 5 Ma, 317 ± 7 Ma and 282 ± 10 Ma, representing the ages of inherited or captured zircons entrained by the granitic magma.

Sample JG-3 (Granodiorite)

Out of thirty analytical spots, 27 analyses from sample JG-3 are concordant and yielded $^{206}\text{Pb}/^{238}\text{U}$ ages from 255 to 250 Ma, which produces a weighted mean age of 253 ± 2 Ma (mean squared weighted deviation (MSWD) = 0.057, $n = 27$; Figure 8c), representing the emplacement age of the granodiorite.

4.2. Zircon Hf Isotopic Compositions

In situ Lu–Hf isotopic compositions were measured in a total of 41 grains from the conglomerate sample JG-6 and 45 grains from the granitic pebble samples (JG-1, JG-2, and JG-3). The results are listed in Table S2 and are shown in Figure 9.

Forty-one detrital zircon Hf spot analyses from the conglomerate sample JG-6 were obtained, which include 38 Paleozoic–Early Mesozoic zircons that have initial $^{176}\text{Hf}/^{177}\text{Hf}$ ratios of 0.282608–0.282999, $\epsilon_{\text{Hf}}(t)$ values of +4.47 to +14.17, single-stage Hf model ages (T_{DM1}) of 891 to 350 Ma, and two-stage Hf model ages (T_{DM2}) of 1146 to 383 Ma. The remaining three Precambrian (2291, 1044, and 802 Ma) zircons yield relatively lower initial

$^{176}\text{Hf}/^{177}\text{Hf}$ ratios of 0.281270–0.282221, with negative $\varepsilon_{\text{Hf}}(t)$ values of -3.78 to -1.65 . The T_{DM1} and T_{DM2} ages of these three zircons are 2701, 1702, and 1436 Ma and 2947, 2104, and 1807 Ma, respectively.

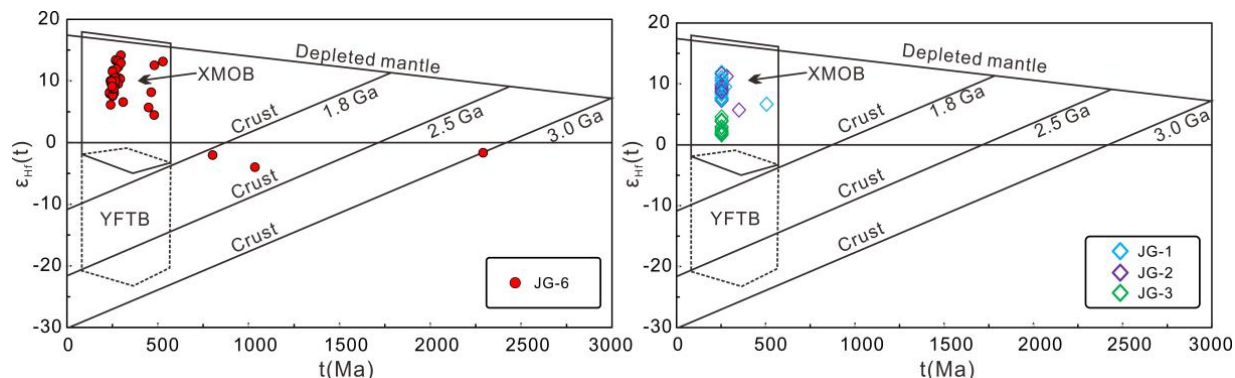


Figure 9. $\varepsilon_{\text{Hf}}(t)$ versus t diagram of the rocks from the Jin'gui Island. XMOB: Xing'an–Mongolia Orogenic Belt; YFTB: Yanshan Fold and Thrust Belt (Yang et al., 2006 [87]).

Forty-five Paleozoic magmatic zircons from the granitic pebble samples were dated for Hf isotopic compositions, with initial $^{176}\text{Hf}/^{177}\text{Hf}$ ratios of 0.282655–0.282954, $\varepsilon_{\text{Hf}}(t)$ values of $+1.61$ to $+11.62$, T_{DM1} values of 829–421 Ma, and T_{DM2} values of 1148–512 Ma, respectively.

4.3. Major and Trace Elements

Five samples, listed in Table 1, were analyzed to know the geochemical features of the Late Permian granitic pebbles from the Jin'gui Island. All the data are plotted in Figures 10 and 11.

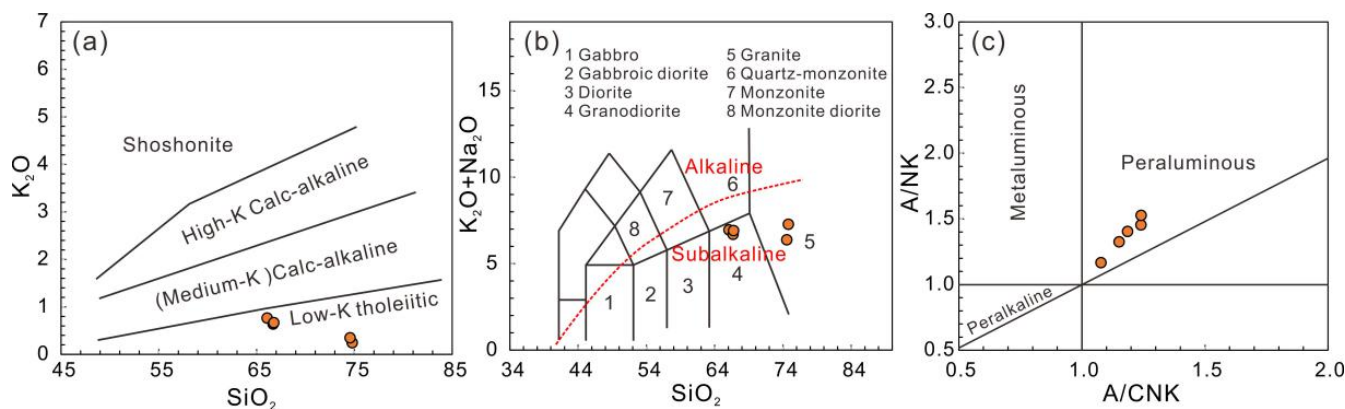


Figure 10. Major element diagrams for the granitic pebbles in the conglomerate. (a) K_2O versus SiO_2 diagram (after Peccerillo and Taylor, 1976 [88]); (b) TAS classification diagram (after Middlemost, 1994 [89]); (c) ANK versus ACNK diagram (after Maniar and Piccoli, 1989 [90]).

The granitic pebble samples from the Jin'gui Island have high SiO_2 (66.07–74.77 wt %) and Al_2O_3 (13.64–16.28 wt %) but display low FeO^{T} (1.67–2.09 wt %) and MgO (0.55–2.05 wt %) contents (Table 1). They show relatively lower K_2O (0.25–0.77 wt %) and higher Na_2O (6.03–7.04 wt %) contents (Table 1), therefore having low $\text{K}_2\text{O}/\text{Na}_2\text{O}$ ratios (0.04–0.12 wt %) and showing low-K calc-alkaline characteristics (Figure 10a). In the total alkali-silica (TAS) diagram (Figure 10b), these samples exhibit subalkaline characteristics and plot in the granodiorite and granite fields. They have high A/CNK ratios (1.08–1.24) and are peraluminous (Figure 10c).

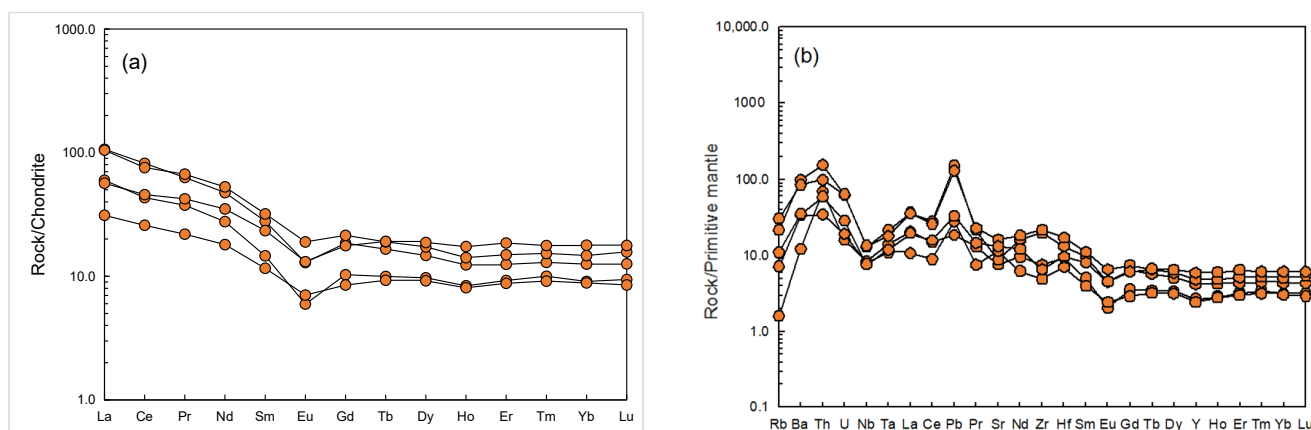


Figure 11. (a) Chondrite-normalized rare earth element (REE) patterns and (b) primitive mantle-normalized trace element patterns of the granitic pebble samples. Normalizing values are from [91].

Table 1. Chemical compositions of major elements (wt %) and trace elements ($\times 10^{-6}$) of the Late Permian granitic pebble samples from the Jin’gui Island.

| Sample | JG-1(1) | JG-1(2) | JG-2(1) | JG-2(2) | JG-3 | Sample | JG-1(1) | JG-1(2) | JG-2(1) | JG-2(2) | JG-3 |
|------------------------------------|---------|---------|---------|---------|--------|----------------------|---------|---------|---------|---------|--------|
| SiO ₂ | 74.77 | 74.55 | 66.07 | 66.67 | 66.75 | Zr | 84.09 | 221.60 | 55.20 | 245.70 | 73.41 |
| Al ₂ O ₃ | 13.82 | 13.64 | 15.99 | 16.28 | 15.44 | Nb | 5.94 | 9.22 | 5.49 | 9.55 | 5.43 |
| TiO ₂ | 0.37 | 0.32 | 0.78 | 0.59 | 0.74 | Cs | 0.24 | 0.96 | 0.63 | 1.19 | 0.70 |
| FeO | 0.85 | 0.89 | 2.37 | 1.43 | 1.18 | Ba | 85.27 | 688.05 | 238.40 | 593.47 | 247.30 |
| Fe ₂ O ₃ | 0.98 | 2.14 | 2.26 | 4.36 | 3.68 | La | 14.19 | 25.20 | 7.38 | 24.80 | 13.42 |
| CaO | 0.54 | 0.85 | 1.04 | 1.35 | 1.12 | Ce | 26.46 | 50.19 | 15.82 | 46.32 | 28.00 |
| MgO | 0.55 | 0.73 | 1.79 | 2.05 | 1.95 | Pr | 3.58 | 5.98 | 2.08 | 6.36 | 4.02 |
| K ₂ O | 0.25 | 0.35 | 0.77 | 0.64 | 0.67 | Nd | 12.92 | 22.20 | 8.43 | 24.70 | 16.36 |
| Na ₂ O | 7.04 | 6.03 | 6.18 | 6.06 | 6.24 | Sm | 2.24 | 4.26 | 1.78 | 4.89 | 3.58 |
| MnO | 0.03 | 0.12 | 0.06 | 0.09 | 0.06 | Eu | 0.35 | 0.75 | 0.41 | 1.10 | 0.76 |
| P ₂ O ₅ | 0.06 | 0.08 | 0.15 | 0.19 | 0.16 | Gd | 2.11 | 3.81 | 1.75 | 4.40 | 3.63 |
| LOI | 0.55 | 1.26 | 1.80 | 2.02 | 1.59 | Tb | 0.37 | 0.62 | 0.35 | 0.71 | 0.72 |
| Total | 99.79 | 100.96 | 99.26 | 101.73 | 99.58 | Dy | 2.47 | 3.74 | 2.34 | 4.39 | 4.77 |
| A/CNK | 1.08 | 1.15 | 1.24 | 1.24 | 1.19 | Ho | 0.47 | 0.70 | 0.46 | 0.80 | 0.98 |
| A/NK | 1.17 | 1.32 | 1.45 | 1.53 | 1.40 | Er | 1.53 | 2.07 | 1.45 | 2.47 | 3.08 |
| σ | 1.67 | 1.29 | 2.09 | 1.90 | 2.01 | Tm | 0.26 | 0.33 | 0.23 | 0.39 | 0.45 |
| FeO ^T | 1.73 | 2.82 | 4.40 | 5.35 | 4.50 | Yb | 1.54 | 2.13 | 1.50 | 2.50 | 3.03 |
| K ₂ O/Na ₂ O | 0.04 | 0.06 | 0.12 | 0.11 | 0.11 | Lu | 0.24 | 0.32 | 0.22 | 0.40 | 0.45 |
| Mg# | 36.02 | 31.61 | 41.95 | 40.57 | 43.64 | Hf | 2.91 | 4.06 | 2.19 | 5.31 | 3.00 |
| Be | 0.77 | 1.26 | 1.00 | 1.82 | 1.23 | Ta | 0.58 | 0.89 | 0.45 | 0.74 | 0.49 |
| Sc | 3.89 | 5.93 | 6.86 | 12.72 | 8.98 | Pb | 3.46 | 28.00 | 5.21 | 24.10 | 6.17 |
| V | 24.68 | 24.20 | 86.40 | 67.70 | 82.60 | Th | 5.91 | 13.20 | 2.98 | 8.42 | 5.03 |
| Cr | 213.50 | 26.30 | 268.40 | 16.10 | 234.10 | U | 0.33 | 1.32 | 0.41 | 1.34 | 0.60 |
| Co | 2.81 | 5.55 | 5.20 | 10.07 | 6.24 | δ Eu | 0.48 | 0.56 | 0.70 | 0.71 | 0.64 |
| Ni | 6.79 | 13.70 | 8.10 | 11.50 | 4.53 | (La/Yb) _N | 9.08 | 12.53 | 8.82 | 14.71 | 17.84 |
| Cu | 14.88 | 36.20 | 8.91 | 20.10 | 9.69 | (La/Sm) _N | 14.63 | 27.84 | 11.60 | 31.96 | 23.41 |
| Zn | 11.69 | 30.40 | 26.04 | 54.20 | 36.60 | (Gd/Yb) _N | 10.28 | 18.54 | 8.50 | 21.41 | 17.68 |
| Ga | 6.83 | 13.50 | 8.24 | 18.20 | 10.25 | Σ REE | 4.09 | 3.82 | 2.68 | 3.27 | 2.42 |
| Rb | 1.02 | 13.80 | 4.55 | 19.40 | 6.98 | Σ LREE | 1.13 | 1.48 | 0.96 | 1.46 | 0.99 |
| Sr | 160.40 | 186.00 | 240.70 | 341.00 | 276.40 | Σ HREE | 6.60 | 8.49 | 3.53 | 7.12 | 3.17 |
| Y | 12.31 | 19.00 | 11.11 | 21.90 | 27.05 | T _{Zr} (°C) | 737 | 820 | 705 | 830 | 727 |

Note: A/CNK = mole [Al₂O₃/(CaO + Na₂O + K₂O)]; A/NK=mole [Al₂O₃/(Na₂O + K₂O)]; δ Eu = $2 \times \text{Eu}_N / (\text{Gd}_N + \text{Sm}_N)$; LREE = La + Ce + Pr + Nd + Sm + Eu; HREE = Gd + Tb + Dy + Ho + Er + Tm + Yb + Lu; Σ REE = Σ LREE + Σ HREE.

With regard to trace elements, the granitic pebble samples have uniform rare earth element (REE) patterns in the chondrite-normalized diagram (Figure 11a) and are characterized by light rare earth element (LREE) enrichment ((La/Yb)_N = 3.17–8.49) and flat

heavy rare earth element (HREE) patterns ($(\text{Gd}/\text{Yb})_N = 0.96\text{--}1.48$) with negative Eu anomalies ($\delta\text{Eu} = 0.48\text{--}0.71$). In the primitive mantle-normalized trace element spider diagrams (Figure 11b), these samples show Nb, Ta, and Ti negative anomalies, and display positive Ba, Th, and Pb spikes, thereby indicating typical characteristics of arc-related magmatic rocks [92–97].

4.4. Sr–Nd Isotopic Analyses

The results of the Sr–Nd isotopic analyses of the granitic pebbles from the Jin’gui Island are listed in Table 2. The initial $^{87}\text{Sr}/^{86}\text{Sr}$ and $\epsilon_{\text{Nd}}(t)$ values were calculated based on their zircon U–Pb ages. For the Late Permian granitic rocks, $(^{87}\text{Sr}/^{86}\text{Sr})_i = 0.706458\text{--}0.706842$ and $\epsilon_{\text{Nd}}(t) = +3.3$ to $+4.2$, and the two-stage Nd model ages (T_{DM2}) range from 758 to 685 Ma. These values are consistent with those of the Phanerozoic felsic rocks in the CAOB [25,39].

Table 2. Sr–Nd isotopic data for the Late Permian granitic pebble samples from the Jin’gui Island.

| Sample | t(Ma) | $^{87}\text{Rb}/^{86}\text{Sr}$ | $^{87}\text{Sr}/^{86}\text{Sr}$ | 2σ | $(^{87}\text{Sr}/^{86}\text{Sr})_i$ | $^{147}\text{Sm}/^{144}\text{Nd}$ | $^{143}\text{Nd}/^{144}\text{Nd}$ | $\pm 2\sigma$ | $\epsilon_{\text{Nd}}(t)$ | $T_{\text{DM2}}(\text{Ma})$ |
|---------|-------|---------------------------------|---------------------------------|-----------|-------------------------------------|-----------------------------------|-----------------------------------|---------------|---------------------------|-----------------------------|
| JG-1(1) | 254 | 0.214835 | 0.707270 | 0.000009 | 0.706494 | 0.116010 | 0.512671 | 0.000006 | 3.3 | 758 |
| JG-2(1) | 253 | 0.164735 | 0.707051 | 0.000009 | 0.706458 | 0.119688 | 0.512724 | 0.000006 | 4.2 | 685 |
| JG-3 | 253 | 0.073123 | 0.707105 | 0.000010 | 0.706842 | 0.132294 | 0.512736 | 0.000005 | 4.0 | 699 |

5. Discussion

5.1. Age Interpretations

The sedimentary rocks on the Jin’gui Island were previously assigned to the Yangjiagou Formation, the depositional period of which has long been a controversial topic, since neither the top nor the bottom surface of the strata has been found [80]. Recent LA-ICP-MS dating documented maximum depositional ages of 262, 264, 258, 254, and 245 Ma for the sandstones from the Yangjiagou Formation in the same/adjacent areas [48–50]. However, the formation age of the conglomerate in the Yangjiagou Formation has not been well constrained.

In the present study, zircons in the granitic pebble samples from the conglomerate display typical oscillatory growth zoning, with high Th/U ratios (0.34–2.06, average 0.92), indicating a magmatic origin. Therefore, we conclude that the LA-ICP-MS U–Pb ages for these zircons represent the emplacement age of the granites. The weighted mean $^{206}\text{Pb}/^{238}\text{U}$ ages for three granitic pebbles are 254 ± 2 Ma, 253 ± 3 Ma, and 253 ± 2 Ma, indicating that the granitic rocks formed in the end-Permian. Consequently, the formation timing of the conglomerate on the Jin’gui Island should be not earlier than the end-Permian. Furthermore, a new youngest, concordant $^{206}\text{Pb}/^{238}\text{U}$ age obtained from sample JG-6 is 231 Ma, which suggests that the age of the conglomerate on the Jin’gui Island is Late Triassic or younger, because a sedimentary unit can be no older than the youngest detrital zircon(s) within that unit [98]. This, combined with presence of the overlying Upper Triassic Sihetun Formation, suggests that the conglomerate on the Jin’gui Island formed during the Late Triassic.

5.2. Petrogenetic Implications for the Granitic Pebble Samples

The granitic pebble samples in this study are peraluminous, with A/CNK between 1.08 and 1.24. They have relatively high content of Na_2O (6.03–7.04 wt %) but low initial $^{87}\text{Sr}/^{86}\text{Sr}$ ratios (0.706458–0.706842) and positive $\epsilon_{\text{Nd}}(t)$ ratios (3.3–4.2) (Tables 1 and 2), which suggest that these rocks may be I-type and/or A-type, but not S-type granites according to the criteria of Chappell (1999) [99] and Chappell and White (2001) [100–102]. Additionally, these rocks are characterized by low contents of Nb (5.43–9.55 ppm), Ta (0.45–0.89 ppm), Y (11.11–27.05 ppm), and Zn (11.69–54.20 ppm) alongside low $10,000 \times \text{Ga}/\text{Al}$ (0.93–2.11) and FeO^T/MgO (2.30–3.86) values (Table 1), similar to the widely distributed I-type granites in NE China [21,22,25,28–30] but distinct from those A-type granites [103].

This result is also supported by the absence of mafic alkaline minerals such as arfvedsonite and riebeckite.

Zircon saturation temperatures (T_{Zr}) calculated from whole-rock compositions can be used to estimate peak melting temperature experienced by magmatic rocks under the prerequisite that zirconium is saturated in the melt [104–107]. In this study, the presence of inherited zircons in the granitic pebble samples indicates that zirconium was saturated in the parent magma and T_{Zr} is thus applicable. The calculated T_{Zr} for the granitic pebble samples are in the range of 705–830. These values are distinctly lower than those of A-type granites (calculated average T_{Zr} values was 839 °C) [104,105] but consistent with those of I-type granites (calculated average T_{Zr} values for fractionated I-type granites and unfractionated I-type granites were 764 and 781 °C, respectively) [106,107], which further suggests that these granitic pebble samples are I-type granites.

The high SiO_2 concentrations and significant enrichment in large ion lithophile elements (LILEs) and depletion in high field strength elements (HFSEs) in the primitive mantle-normalized multi-element diagram (Figure 11) imply that the primary magma of the above I-type granitic rocks was derived from the partial melting of crustal material [21,22,25,28–30]. The higher SiO_2 but lower MgO and Mg# of these rocks are similar to those of the experimentally derived partial melts from metabasaltic rocks [108]. This, combined with the negative Nb-Ta-Ti anomalies suggests residues of garnet and hornblende in the source [109]. In addition, the granitic samples display low initial $^{87}\text{Sr}/^{86}\text{Sr}$ ratios (0.706458–0.706842), positive $\epsilon_{\text{Nd}}(t)$ (3.3–4.2) and zircon $\epsilon_{\text{Hf}}(t)$ (1.61–11.62) values, and young second-stage Hf model ages from 1148 to 512 Ma, which are consistent with the isotopic features of widely distributed Permian felsic igneous rocks along the CYS and indicate crustal growth during the Meso–Neoproterozoic [21,22,25,28–30]. Therefore, the primary magma of the I-type granitic pebble samples from the Jin'gui Island likely originated from the partial melting of a Meso–Neoproterozoic juvenile metabasaltic lower crust, with garnet and hornblende as the major residue mineral phases in the source region.

5.3. Provenance Analysis of the Conglomerate on the Jin'gui Island

It is widely accepted that age dating and Hf compositions of detrital zircon is a proven and effective method in determining the provenance of clastic sedimentary rocks [42–50,110–112]. Apart from three zircon grains that yield Paleoproterozoic (2291 Ma), Mesoproterozoic (1044 Ma), and Neoproterozoic (802 Ma) ages, the remaining 225 detrital zircons from the conglomerate analyzed in this study yield two populations: 529–426 Ma (Early Paleozoic) with a peak at 473 Ma and 334–231 Ma (Late Paleozoic–Early Mesozoic) with a peak at 254 Ma (Figure 6b). Therefore, the material deposited within the Late Triassic conglomerate on the Jin'gui Island was predominantly derived from a Paleozoic–Early Mesozoic source, with minor contributions from Paleoproterozoic to Neoproterozoic sources.

The Paleoproterozoic (2291 Ma) zircon has a negative $\epsilon_{\text{Hf}}(t)$ value of -1.65 , which is similar to Precambrian detrital and magmatic zircons from the NCC [16–19,42–50]. This suggests that the Paleoproterozoic zircon was sourced from Precambrian basement rocks of the NCC. In addition, this zircon is rounded in shape, indicating that it underwent long distance transportation prior to deposition.

The NCC experienced the Columbia supercontinental final break at approximately 1.35–1.32Ga, leading to absence of the Grenvillian (≈ 1200 –800 Ma) magmatic events in the NCC, especially in the northern margin [113,114]. Therefore, it is impossible that the source region of the Mesoproterozoic and Neoproterozoic zircons was the NCC. In contrast, the two zircons have negative $\epsilon_{\text{Hf}}(t)$ values and are similar to those Mesoproterozoic–Neoproterozoic isotopic ages identified in the Xing'an–Mongolian Orogenic Belt (XMOB) [115,116], suggesting that they were derived from microcontinents to the north [44].

The Early Paleozoic and Late Paleozoic–Early Mesozoic zircons display the characteristics of magmatic zircons, indicating intense magmatic activity during these periods. As a result of initial and ongoing subduction of the Paleo-Asian oceanic plate, an Early Paleozoic intra-oceanic arc abutting the northern margin of the NCC was proposed [117].

This view is supported by some Early Paleozoic mid-ocean ridge basalt (MORB)-like and arc-like magmatic rocks identified in the study area and adjacent regions, including the Zhangjiatun meta-diabase dyke (493 Ma), hornblende gabbro (486 Ma), quartz diorite (476 Ma), and tonalite (443 and 440 Ma) [117,118]; the Xiaosuihe serpentinite (494 Ma) and pyroxene andesite (467 Ma) [118]; the Toudaogou metamorphic intermediate-mafic and ultramafic rocks (474, 468, 466, and 465 Ma) [13]; and the Fangniugou rhyodacite (425 Ma) [12]. In addition, the Early Paleozoic zircons in the conglomerate have positive $\epsilon_{\text{Hf}}(t)$ values (Figure 9a), similar to those in the above magmatic rocks but distinct from the Phanerozoic zircons from the NCC that generally have negative $\epsilon_{\text{Hf}}(t)$ values [87]. Moreover, these zircons are subhedral–euhedral in shape, indicating that they underwent minimal transportation prior to deposition. Thus, zircons with ages of 529–426 Ma were most likely derived from the Early Paleozoic arc at the northern margin of the NCC.

The Late Paleozoic–Early Mesozoic zircons also display the characteristics of magmatic zircons and are subhedral–euhedral in shape, indicating that they were locally derived from magmatic rocks. The 16 zircons with ages of 334–300 Ma closely match the ages recorded in Permian–Triassic strata (e.g., the Shoushangou, Fanjiatun, Yangjiagou, Huangyingtun, Dongnancha, Xiaohekou and Dajianggang formations) in central Jilin Province [43,44,46–50]. The 87 Permian–Triassic (298–231 Ma) zircons are commonly recorded from the widely distributed magmatic rocks in the study area and adjacent regions, including the Daheshen volcanic rocks (299 Ma) [39]; the Fangniugou monzogranite (270 Ma) [21]; the Xiaolihe monzogranite (260 Ma) [22]; the Youyi syenogranite (259 Ma) [21]; the Shuangfengshan olivine gabbro (258 Ma) [21]; the Fangshendingzi monzogabbro (257 Ma) [21]; the Doushantouzi syenogranite (257 Ma) [25]; the Sanmenmojia granodiorite (255 Ma) [21]; the Daheishan volcanic rocks (255–253 Ma) [25]; the Shanhe monzonite (252 Ma) [22]; the Tuding hornblende gabbro (252 Ma) [22]; the Jianpingzhen monzogranite (249 Ma) [21]; the Nantiancun granodiorite (235 Ma) [20]. In addition, all the Late Paleozoic–Early Mesozoic zircons have positive $\epsilon_{\text{Hf}}(t)$ values (Figure 9a), which are similar to the compositions of zircons in the above sedimentary and magmatic rocks. Therefore, zircons with ages of 334–231 Ma were locally derived from the Late Paleozoic–Early Mesozoic sedimentary and magmatic rocks in the study area and adjacent regions.

In summary, the provenance of the conglomerate on Jin’gui Island was mainly the Early Paleozoic magmatic arc and Late Paleozoic–Early Mesozoic sedimentary and magmatic rocks in the study area and adjacent regions, and to a lesser degree the interior of the NCC and the XMOB.

5.4. Implications for the Tectonic Evolution of the PAO

As stated above, the timing of the final closure of the eastern segment of the PAO has been controversial, and various dominant views have indicated that the final closure of the PAO occurred during the late Early Permian [60,61], the Middle–Late Permian [62–65], the Late Permian [4,34,48,66], the Late Permian–Early Triassic [3,10,11,21,33,35,40,41,50,67–70], the Late Permian–Middle Triassic [5,22,25,26,28,32,42,71,72], and the Middle–Late Triassic [20,24,37,49,73]. The determination of the age of the molasse deposits on the Jin’gui Island provides new evidence for in-depth understanding of the Late Permian–Late Triassic tectonic evolution of the PAO.

The petrological and geochemical data show that the Late Permian granitic pebbles were formed by partial melting of the lower crustal-derived juvenile component. They display depletion in HFSEs and LILEs enrichment, and they also have low initial $^{87}\text{Sr}/^{86}\text{Sr}$ ratios and positive $\epsilon_{\text{Nd}}(t)$ values, which are akin to representative island arc-like magmas [119]. In addition, all the granitic samples plot within the field of volcanic arc granite within the Ta vs. Yb and Rb vs. Y + Nb discrimination diagrams (Figure 12a,b), suggesting that they were generated in an arc-related tectonic setting. Moreover, all the samples plot within or close to the typical arc-rock field in the Sr/Y vs. Y and $(\text{La}/\text{Yb})_{\text{N}}$ vs. Yb diagrams (Figure 12c,d), which are further indicative of arc-type magmatism in association with subduction process. Therefore, a subduction-related tectonic setting linking with the sub-

duction of the Paleo-Asian oceanic plate likely created the above-mentioned end-Permian granitic rocks, as well as some previously reported contemporaneous magmatic rocks, which exhibit arc-related geochemical signatures along the CYS, such as the Doushantouzi syenogranites (256 Ma), the Daheishan volcanic rocks (255–253 Ma), the Kaiyuan metamorphosed basaltic volcanic rocks (258 Ma and 254 Ma), and the Kaishantun basalt (252 Ma) [17,25,26,31]. In addition, coeval high-Mg andesites (252 Ma and 250 Ma) that formed in a subduction-related setting also distributed along the CYS [23,34]. Thus, we conclude that the eastern segment of the PAO was undergoing subduction in the end-Permian, implying that the PAO still existed along the southeastern margin of the XMOB in the end-Permian.

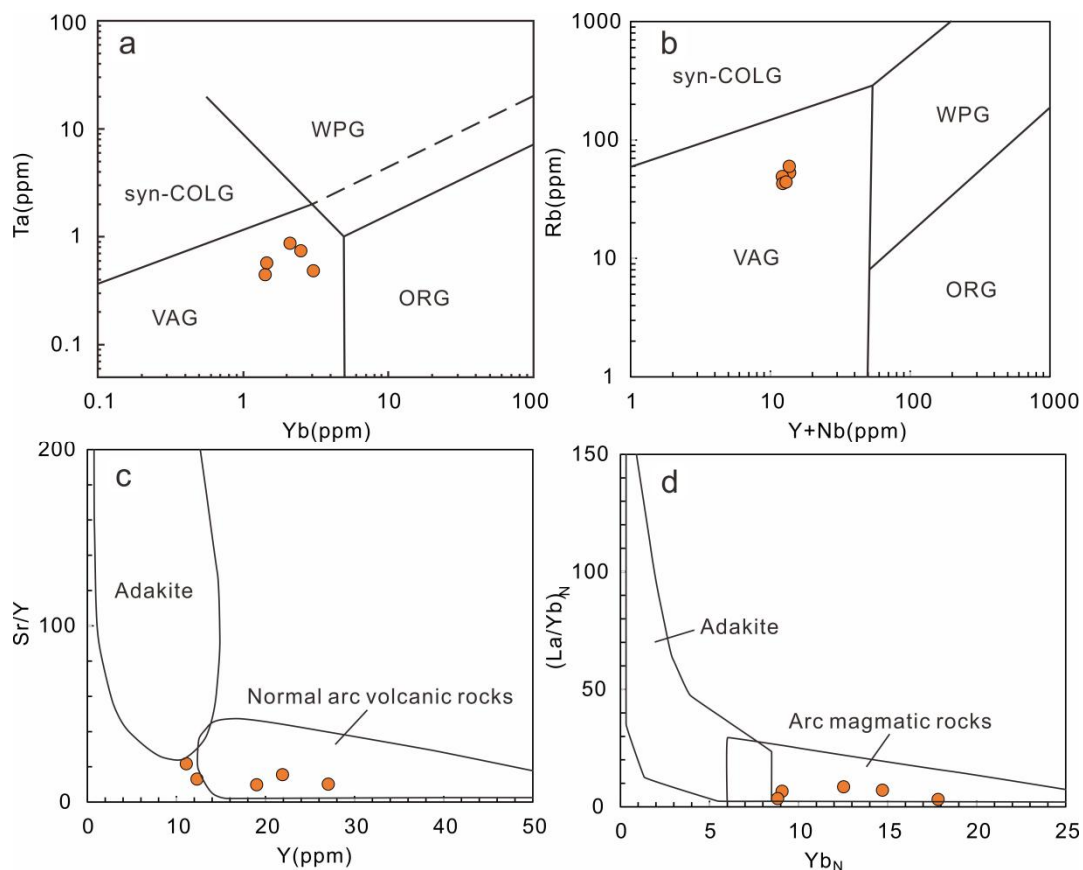


Figure 12. (a) Ta versus Yb diagram (after Pearce et al., 1984 [120]) (b) Rb versus Y+Nb diagram (after Whalen et al., 1987 [103]), (c) Sr/Y versus Y diagram (after Defant and Drummond, 1990 [121]), and (d) $(La/Yb)_N$ versus Yb_N diagram (after Martin et al., 2005 [122]) for the granitic pebble samples. Abbreviations: syn-COLG, syn-collision granite; WPG, within plate granite; ORG, ocean ridge granite; VAG, volcanic arc granite.

The occurrences of many Early Triassic syn-collisional granitoids (such as the Jianpingzhen, Liushugou, Dayushan, and Fudongzhen plutons) along the CYS record the collisional events between the NCC and combined NE China blocks [20–22,24,27,28]. These granitoids, which display high SiO_2 , low Mg#, low Cr and Ni, and notably high La/Yb and Sr/Y, were proposed to have originated from thickened lower crust that resulted from collision [20–22,24,27,28]. Some recently reported Early Triassic ages from igneous rocks or metamorphic complexes (e.g., the Daheishan volcanic rocks and the Kaiyuan and Hulan complexes) in the adjacent areas probably correspond to the above collisional events [10,25,26,31]. Importantly, molasse sequences provide reliable evidence for the end of an orogeny [5,46]. The identification of Late Triassic molasse deposits on the Jin'gui Island in this study, together with previously identified contemporaneous molasse sequences in the adjacent regions along the CYS (e.g., the Xiaohekou, Xiaoyngzi, and Dajianggang

formations), indicates that final closure of the PAO took place prior to the Late Triassic [46]. Considering the above, we suggest that final suturing of the eastern segment of the PAO took place during the Early–Middle Triassic in central Jilin Province.

6. Conclusions

Our new geochemical and geochronological data for the granitic pebbles and conglomerate from molasse deposits of the Jin’gui Island in NE China led us to the following conclusions.

- (1) The zircon U-Pb data indicate that the granitic pebbles included in the conglomerate formed in the end-Permian (254–253 Ma). The youngest detrital zircon age of 231 Ma from the conglomerate on the Jin’gui Island, together with the overlying Upper Triassic Sihetun Formation, indicates that the molasse deposits formed during the Late Triassic.
- (2) The primary magma of the end-Permian granitic pebble samples was derived from the partial melting of a Meso-Neoproterozoic juvenile metabasaltic lower crust.
- (3) The provenance of the conglomerate on the Jin’gui Island was mainly the Early Paleozoic magmatic arc and Late Paleozoic–Early Mesozoic sedimentary and magmatic rocks in the study area and adjacent regions, and to a lesser degree the interior of the NCC and the XMOB.
- (4) The end-Permian granitic pebbles on the Jin’gui Island represent the final stages of arc magmatism related to subduction of the Paleo-Asian oceanic plate. These rocks, together with the identification of Late Triassic molasse deposits along the CYS, suggest that the final closure of the PAO in central Jilin Province occurred during the Early–Middle Triassic.

Supplementary Materials: The following are available online at <https://www.mdpi.com/2075-163X/11/2/223/s1>, Table S1: LA-ICP-MS zircon U-Pb data for the samples from the Jin’gui Island, Table S2: Lu-Hf isotopic data of zircons from the samples from the Jin’gui Island. References [25,123–128] are cited in the supplementary materials.

Author Contributions: Conceptualization, Z.H., Sampling and Experiments, J.L., W.Z., Z.S., and Z.H., Data analysis and Figures, J.L., W.Z., C.Z., and Z.S., Writing—Original Draft Preparation, Z.S., Writing—Review and Editing, Z.H. and J.L., All authors have read and agreed to the published version of the manuscript.

Funding: This research was funded by the Natural Science Foundation of Shandong Province (Grant ZR2019PD001), the Taishan Scholar Talent Team Support Plan for Advantaged & Unique Discipline Areas, the Youth Innovation Team Development Plan of Universities in Shandong Province (Deep-Time Paleoclimate and Sedimentary Mineralization), and the SDUST Research Fund (Grant 2015TDJH101).

Data Availability Statement: Data are contained within the article and Supplementary Tables.

Acknowledgments: We acknowledge the help of Yujing Peng, Zhiping Guo, Guyao Liu, Mei Han, Junlei Yan and Lihua Gao, who participated in the field work. Many thanks to the editor and two anonymous reviewers for their helpful and constructive reviews.

Conflicts of Interest: The authors declare no conflict of interest.

References

1. Şengör, A.M.C.; Natal’in, B.A.; Burtman, V.S. Evolution of the Altaid tectonic collage and Palaeozoic crustal growth in Eurasia. *Nature* **1993**, *364*, 299–307. [[CrossRef](#)]
2. Jahn, B. The Central Asian Orogenic Belt and growth of the continental crust in the Phanerozoic. *Geol. Soc. Lond. Spec. Publ.* **2004**, *226*, 73–100. [[CrossRef](#)]
3. Xiao, W.J.; Windley, B.; Sun, S.; Li, J.L.; Huang, B.C.; Han, C.M.; Yuan, C.; Sun, M.; Chen, H.L. A tale of amalgamation of three Permo–Triassic collage systems in Central Asia: Oroclines, sutures, and terminal accretion. *Annu. Rev. Earth Planet. Sci.* **2015**, *43*, 477–507. [[CrossRef](#)]

4. Li, J.Y. Permian geodynamic setting of northeast China and adjacent regions: Closure of the Paleo-Asian Ocean and subduction of the Paleo-Pacific plate. *J. Asian Earth Sci.* **2006**, *26*, 207–224. [[CrossRef](#)]
5. Liu, Y.J.; Li, W.M.; Feng, Z.Q.; Wen, Q.B.; Neubauer, F.; Liang, C.Y. A review of the Paleozoic tectonics in the eastern part of Central Asian Orogenic Belt. *Gondwana Res.* **2017**, *43*, 123–148. [[CrossRef](#)]
6. Du, Q.X.; Han, Z.Z.; Shen, X.L.; Han, C.; Han, M.; Song, Z.G.; Gao, L.H.; Liu, H.; Zhong, W.J.; Yan, J.L. Zircon U–Pb geochronology and geochemistry of the post-collisional volcanic rocks in eastern Xinjiang Province, NW China: Implications for the tectonic evolution of the Junggar terrane. *Int. Geol. Rev.* **2018**, *60*, 339–364. [[CrossRef](#)]
7. Han, Z.Z.; Liu, H.; Song, Z.G.; Zhong, W.J.; Han, C.; Han, M.; Du, Q.X.; Gao, L.H.; Li, J.J.; Yan, J.L. Geochronology, geochemistry, and tectonic implications of upper Silurian–Lower Devonian meta-sedimentary rocks from the Jiangyu group in eastern Jilin Province, Northeast China. *Can. J. Earth Sci.* **2018**, *55*, 490–504. [[CrossRef](#)]
8. Zhou, J.B.; Wilde, S.A.; Zhao, G.C.; Han, J. Nature and assembly of microcontinental blocks within the Paleo-Asian Ocean. *Earth-Sci. Rev.* **2018**, *186*, 76–93. [[CrossRef](#)]
9. Wu, F.Y.; Jahn, B.M.; Wilde, S.; Sun, D.Y. Phanerozoic crustal growth: U–Pb and Sr–Nd isotopic evidence from the granites in northeastern China. *Tectonophysics* **2000**, *328*, 89–113. [[CrossRef](#)]
10. Wu, F.Y.; Zhao, G.C.; Sun, D.Y.; Wilde, S.A.; Yang, J.H. The Hulan Group: Its role in the evolution of the Central Asian Orogenic Belt of NE China. *J. Asian Earth Sci.* **2007**, *30*, 542–556. [[CrossRef](#)]
11. Wilde, S.A. Final amalgamation of the Central Asian Orogenic Belt in NE China: Paleo-Asian Ocean closure versus Paleo-Pacific plate subduction—A review of the evidence. *Tectonophysics* **2015**, *662*, 345–362. [[CrossRef](#)]
12. Han, Z.Z.; Song, Z.G.; Han, C.; Zhong, W.J.; Han, M.; Yan, J.L.; Liu, H.; Du, Q.X.; Gao, L.H.; Li, J.J. U–Pb ages and Hf isotopic composition of zircons and whole rock geochemistry of volcanic rocks from the Fangniugou area: Implications for early–middle Paleozoic tectonic evolution in Jilin Province, NE China. *J. Miner. Petrol. Sci.* **2018**, *113*, 10–23. [[CrossRef](#)]
13. Song, Z.G.; Han, C.; Liu, H.; Han, Z.Z.; Yan, J.L.; Zhong, W.J.; Gao, L.H.; Du, Q.X.; Han, M.; Li, J.J. Early-Middle Ordovician intermediate-mafic and ultramafic rocks in central Jilin Province, NE China: Geochronology, origin, and tectonic implications. *Miner. Petrol.* **2019**, *113*, 393–415. [[CrossRef](#)]
14. Pang, Y.M.; Guo, X.W.; Zhang, X.H.; Zhu, X.Q.; Hou, F.H.; Wen, Z.H.; Han, Z.Z. Late Mesozoic and Cenozoic tectono-thermal history and geodynamic implications of the Great Xing’an Range, NE China. *J. Asian Earth Sci.* **2020**, *189*, 104155. [[CrossRef](#)]
15. Han, Z.Z.; Ren, X.; Schertl, H.P.; Li, X.P.; Song, Z.G.; Du, Q.X.; Han, C.; Zhong, W.J.; Gao, L.H. Zircon U–Pb–Hf isotopes and geochemistry of Jurassic igneous rocks from the southern Zhangguangcai Range, NE China: Constraints on magmatism, petrogenesis and tectonic implications. *Int. Geol. Rev.* **2020**, *62*, 1988–2012. [[CrossRef](#)]
16. Du, Q.X.; Han, Z.Z.; Shen, X.L.; Han, C.; Song, Z.G.; Gao, L.H.; Han, M.; Zhong, W.J.; Yan, J.L. New evidence of detrital zircon ages for the final closure time of the Paleo-Asian Ocean in the eastern Central Asian Orogenic Belt (NE China). *Acta Geol. Sin. Engl. Ed.* **2017**, *91*, 1910–1914. [[CrossRef](#)]
17. Du, Q.X.; Han, Z.Z.; Shen, X.L.; Gao, L.H.; Han, M.; Song, Z.G.; Li, J.J.; Zhong, W.J.; Yan, J.L.; Liu, H. Geochemistry and geochronology of Upper Permian–Upper Triassic volcanic rocks in eastern Jilin Province, NE China: Implications for the tectonic evolution of the Palaeo-Asian Ocean. *Int. Geol. Rev.* **2017**, *59*, 368–390. [[CrossRef](#)]
18. Du, Q.X.; Han, Z.Z.; Shen, X.L.; Han, C.; Song, Z.G.; Gao, L.H.; Han, M.; Zhong, W.J. Geochronology and geochemistry of Permo-Triassic sandstones in eastern Jilin Province (NE China): Implications for final closure of the Paleo-Asian Ocean. *Geosci. Front.* **2019**, *10*, 368–390. [[CrossRef](#)]
19. Shen, X.L.; Du, Q.X.; Han, Z.Z.; Song, Z.G.; Han, C.; Zhong, W.J.; Ren, X. Constraints of zircon U–Pb–Hf isotopes from Late Permian–Middle Triassic flora-bearing strata in the Yanbian area (NE China) on a scissor-like closure model of the Paleo-Asian Ocean. *J. Asian Earth Sci.* **2019**, *183*, 103964. [[CrossRef](#)]
20. Guan, Q.B.; Liu, Z.H.; Liu, Y.J.; Li, S.Z.; Wang, S.J.; Chen, Z.X.; Zhang, C. A Tectonic Transition from Closure of the Paleo-Asian Ocean to Subduction of the Paleo-Pacific Plate: Insights from Early Mesozoic Igneous Rocks in Eastern Jilin Province, NE China. Available online: <https://doi.org/10.1016/j.gr.2020.05.001> (accessed on 8 May 2020).
21. Cao, H.H.; Xu, W.L.; Pei, F.P.; Wang, Z.W.; Wang, F.; Wang, Z.J. Zircon U–Pb geochronology and petrogenesis of the Late Paleozoic–Early Mesozoic intrusive rocks in the eastern segment of the northern margin of the North China Block. *Lithos* **2013**, *170–171*, 191–207. [[CrossRef](#)]
22. Wang, Z.J.; Xu, W.L.; Pei, F.P.; Wang, Z.W.; Li, Y.; Cao, H.H. Geochronology and geochemistry of middle Permian–Middle Triassic intrusive rocks from central-eastern Jilin Province, NE China: Constraints on the tectonic evolution of the eastern segment of the Paleo-Asian Ocean. *Lithos* **2015**, *238*, 13–25. [[CrossRef](#)]
23. Yuan, L.L.; Zhang, X.H.; Xue, F.H.; Lu, Y.H.; Zong, K.Q. Late Permian high-Mg andesite and basalt association from northern Liaoning, North China: Insights into the final closure of the Paleo-Asian ocean and the orogeny-craton boundary. *Lithos* **2016**, *258–259*, 58–76. [[CrossRef](#)]
24. Yang, D.G.; Sun, D.Y.; Gou, J.; Hou, X.G. U–Pb ages of zircons from Mesozoic intrusive rocks in the Yanbian area, Jilin Province, NE China: Transition of the Paleo-Asian oceanic regime to the circum-Pacific tectonic regime. *J. Asian Earth Sci.* **2017**, *143*, 171–190. [[CrossRef](#)]
25. Song, Z.G.; Han, Z.Z.; Gao, L.H.; Geng, H.Y.; Li, X.P.; Meng, F.X.; Han, M.; Zhong, W.J.; Li, J.J.; Du, Q.X.; et al. Permo-Triassic evolution of the southern margin of the Central Asian Orogenic Belt revisited: Insights from Late Permian igneous suite in the Daheishan Horst, NE China. *Gondwana Res.* **2018**, *56*, 23–50. [[CrossRef](#)]

26. Guan, Q.B.; Liu, Z.H.; Liu, Y.J.; Liu, J.; Wang, S.J.; Tian, Y. Geochemistry and zircon U–Pb geochronology of mafic rocks in the Kaiyuan tectonic mélange of northern Liaoning Province, NE China: Constraints on the tectonic evolution of the Paleo-Asian Ocean. *Geol. J.* **2019**, *54*, 656–678. [[CrossRef](#)]
27. Shi, Y.; Liu, Z.H.; Liu, Y.J.; Shi, S.S.; Wei, M.H.; Yang, J.J.; Gao, T. Late Paleozoic–Early Mesozoic southward subduction-closure of the Paleo-Asian Ocean: Proof from geochemistry and geochronology of Early Permian–Late Triassic felsic intrusive rocks from North Liaoning, NE China. *Lithos* **2019**, *346–347*, 105165. [[CrossRef](#)]
28. Liu, J.; Zhang, J.; Liu, Z.H.; Yin, C.Y.; Zhao, C.; Yu, X.Y.; Chen, Y.; Tian, Y.; Dong, Y. Petrogenesis of Permo-Triassic intrusive rocks in Northern Liaoning Province, NE China: Implications for the closure of the eastern Paleo-Asian Ocean. *Int. Geol. Rev.* **2020**, *62*, 754–780. [[CrossRef](#)]
29. Jing, Y.; Ge, W.C.; Dong, Y.; Yang, H.; Ji, Z.; Bi, J.H.; Zhou, H.Y.; Xing, D.H. Early–Middle Permian southward subduction of the eastern Paleo-Asian Ocean: Constraints from geochronology and geochemistry of intermediate-acidic volcanic rocks in the northern margin of the North China Craton. *Lithos* **2020**, *364–365*, 105491. [[CrossRef](#)]
30. Jing, Y.; Ji, Z.; Ge, W.C.; Dong, Y.; Yang, H.; Bi, J.H. Middle–Late Permian I-Type Granitoids from the Diaobingshan Region in the Northern Margin of the North China Craton: Insight into Southward Subduction of the Paleo–Asian Ocean. Available online: <https://doi.org/10.1080/00206814.2020.1712556> (accessed on 4 January 2020).
31. Han, Z.Z.; Li, J.J.; Song, Z.G.; Liu, G.Y.; Zhong, W.J.; Gao, L.H.; Du, Q.X. Geochemistry and Zircon U–Pb–Hf Isotopes of Metamorphic Rocks from the Kaiyuan and Hulan Tectonic Mélanges, NE China: Implications for the Tectonic Evolution of the Paleo-Asian and Mudanjiang Oceans. *Minerals* **2020**, *10*, 836. [[CrossRef](#)]
32. Chen, C.; Ren, Y.S.; Wu, T.T.; Yang, Q.; Shang, Q.Q. Genesis and mineralization age of the quartz-vein-type scheelite deposits in Eastern Yanbian, Northeast China: Constraints on the regional tectonic setting. *Geol. J.* **2019**, *54*, 639–655. [[CrossRef](#)]
33. Ma, X.H.; Zhu, W.P.; Zhou, Z.H.; Qiao, S.L. Transformation from Paleo-Asian Ocean closure to Paleo-Pacific subduction: New constraints from granitoids in the eastern Jilin–Heilongjiang Belt, NE China. *J. Asian Earth Sci.* **2017**, *144*, 261–286. [[CrossRef](#)]
34. Ma, X.H.; Chen, C.J.; Zhao, J.X.; Qiao, S.L.; Zhou, Z.H. Late Permian intermediate and felsic intrusions in the eastern Central Asian Orogenic Belt: Final-stage magmatic record of Paleo-Asian Oceanic subduction? *Lithos* **2019**, *326–327*, 265–278. [[CrossRef](#)]
35. Shi, C.L.; Ding, X.Z.; Liu, Y.X.; Zhou, X.D.; Nie, L.J. Zircon U–Pb Geochronology and Petrogenesis of Early–Middle Permian Arc-Related Volcanic Rocks in Central Jilin: Implications for the Tectonic Evolution of the Eastern Segment of Central Asian Orogenic Belt. *Acta Geol. Sin. Engl. Ed.* **2020**, *94*, 1207–1222. [[CrossRef](#)]
36. Tang, J.; Li, A.P.; Xu, W.L. Geochronology and geochemistry of late Carboniferous–Middle Jurassic magmatism in the Helong area, NE China: Implications for the tectonic transition from the Paleo-Asian oceanic to circum-Pacific regime. *Geol. J.* **2020**, *55*, 1808–1825. [[CrossRef](#)]
37. Wang, F.; Xu, W.L.; Xing, K.C.; Wang, Y.N.; Zhang, H.H.; Wu, W.; Sun, C.Y.; Ge, W.C. Final Closure of the Paleo-Asian Ocean and Onset of Subduction of Paleo-Pacific Ocean: Constraints from Early Mesozoic Magmatism in Central Southern Jilin Province, NE China. *J. Geophys. Res. Sol. Earth* **2019**, *124*, 2601–2622. [[CrossRef](#)]
38. Wutiepu, W.; Yang, Y.C.; Han, S.J.; Guo, Y.F.; Nie, S.J.; Liu, C.; Fan, W.L. Zircon U–Pb age, Hf isotope, and geochemistry of Late Permian to Triassic igneous rocks from the Jiapigou gold ore belt, NE China: Petrogenesis and tectonic implications. *Geol. J.* **2020**, *55*, 501–516. [[CrossRef](#)]
39. Yu, Q.; Ge, W.C.; Yang, H.; Zhao, G.C.; Zhang, Y.L.; Su, L. Petrogenesis of late Paleozoic volcanic rocks from the Daheshen Formation in central Jilin Province, NE China, and its tectonic implications: Constrains from geochronology, geochemistry and Sr–Nd–Hf isotopes. *Lithos* **2014**, *192–195*, 116–131. [[CrossRef](#)]
40. Zhang, C.; Neubauer, F.; Liu, Z.H.; Cui, F.H.; Guan, Q.B. Final-Stage Magmatic Record of Paleo-Asian Oceanic Subduction? Insights from Late Permian to Early Triassic Intrusive Rocks in the Yanbian Area, Easternmost Central Asian Orogenic Belt. *Minerals* **2020**, *10*, 799. [[CrossRef](#)]
41. Zhao, T.F.; Peng, B.; Sun, F.Y. The closure time of the easternmost segment of the Solonker–Xar Moron–Changchun–Yanji Suture: Determined by the Yangjin’gou Granite Porphyry in the Hunchun Region, northeast China. *Geosci. J.* **2019**, *23*, 933–949. [[CrossRef](#)]
42. Liu, J.; Liu, Z.H.; Zhao, C.; Wang, C.J.; Guan, Q.B.; Dou, S.Y.; Song, S. Geochemistry and U–Pb detrital zircon ages of late Permian to Early Triassic metamorphic rocks from northern Liaoning, North China: Evidence for the timing of final closure of the Paleo-Asian Ocean. *J. Asian Earth Sci.* **2017**, *145*, 460–474. [[CrossRef](#)]
43. Zhou, Z.B.; Pei, F.P.; Wang, Z.W.; Cao, H.H.; Xu, W.L.; Wang, Z.J.; Zhang, Y. Using detrital zircons from late Permian to Triassic sedimentary rocks in the south-eastern Central Asian Orogenic Belt (NE China) to constrain the timing of the final closure of the Paleo-Asian Ocean. *J. Asian Earth Sci.* **2017**, *144*, 82–109. [[CrossRef](#)]
44. Han, Z.Z.; Zhong, W.J.; Song, Z.G.; Han, C.; Han, M.; Gao, L.H.; Du, Q.X.; Li, J.J.; Yan, J.L.; Liu, H. Geochronology and geochemistry of metasedimentary rocks from the Dongnancha Formation in the Huadian area, central Jilin Province, Northeast (NE) China: Implications for the tectonic evolution of the eastern segment of the Paleo-Asian Ocean. *Geochemistry* **2019**, *79*, 94–112. [[CrossRef](#)]
45. Shi, C.L.; Ding, X.Z.; Liu, Y.X.; Zhou, X.D. Detrital-zircon geochronology and Hf isotope of Paleozoic sedimentary rocks in the Jilin Province, NE China: Tectonic significance for microcontinental blocks of eastern Central Asian Orogenic Belt. *Geosci. J.* **2019**, *23*, 707–729. [[CrossRef](#)]

46. Wang, B.; Zhou, J.B.; Wilde, S.A.; Zhang, X.Z.; Ren, S.M. The timing of final closure along the Changchun–Yanji suture zone: Constraints from detrital zircon U–Pb dating of the Triassic Dajianggang Formation, NE China. *Lithos* **2016**, *261*, 216–231. [[CrossRef](#)]
47. Cao, J.L.; Zhou, J.B.; Li, L. The tectonic evolution of the Changchun–Yanji suture zone: Constraints of zircon U–Pb ages of the Yantongshan accretionary complex (NE China). *J. Asian Earth Sci.* **2020**, *194*, 104110. [[CrossRef](#)]
48. Wang, Z.J.; Xu, W.L.; Pei, F.P.; Wang, Z.W.; Li, Y. Geochronology and provenance of detrital zircons from late Palaeozoic strata of central Jilin Province, Northeast China: Implications for the tectonic evolution of the eastern Central Asian Orogenic Belt. *Int. Geol. Rev.* **2015**, *57*, 211–228. [[CrossRef](#)]
49. Zhang, Q.; Liang, C.Y.; Liu, Y.J.; Zheng, C.Q.; Li, W.M. Final Closure Time of the Paleo-Asian Ocean: Implication from the Provenance Transformation from the Yangjiagou Formation to Lujiatun Formation in the Jiutai Area, NE China. *Acta Geol. Sin. Engl. Ed.* **2019**, *93*, 1456–1476. [[CrossRef](#)]
50. Shi, C.L.; Ding, X.Z.; Liu, Y.X.; Zhou, X.D. Detrital zircon U–Pb dating and Hf isotope study of late Palaeozoic sedimentary rocks in central–eastern Jilin Province, NE China: Constraints for tectonic evolution of the eastern segment of the Paleo-Asian Ocean. *Geol. J.* **2020**, *55*, 2717–2737. [[CrossRef](#)]
51. Liu, C.; Zhu, G.; Xie, C.L.; Zhang, S.; Li, Y.J.; Su, N.; Xiao, S.Y. Location and sinistral displacement of the eastern Liaoyuan Accretionary Belt along the Tan–Lu Fault Zone, NE China. *J. Asian Earth Sci.* **2019**, *172*, 409–422. [[CrossRef](#)]
52. Gu, C.C.; Zhu, G.; Li, Y.J.; Su, N.; Xiao, S.Y.; Zhang, S.; Liu, C. Timing of deformation and location of the eastern Liaoyuan Terrane, NE China: Constraints on the final closure time of the Paleo-Asian Ocean. *Gondwana Res.* **2018**, *60*, 194–212. [[CrossRef](#)]
53. Zhou, Z.Z.; Li, S.Z.; Guo, L.L.; Li, X.Y.; Jiang, Z.X.; Liu, Y.J.; Li, Y.; Wang, G.Z.; Lan, H.Y.; Guo, R.H.; et al. Palaeomagnetic assessment of tectonic rotation in Northeast Asia: Implications for the coupling of intracontinental deformation and mantle convection. *Int. Geol. Rev.* **2020**, *62*, 2166–2188. [[CrossRef](#)]
54. Zhao, P.; Chen, Y.; Xu, B.; Faure, M.; Shi, G.Z.; Choulet, F. Did the Paleo–Asian Ocean between north China block and Mongolia block exist during the late Paleozoic? First paleomagnetic evidence from central–eastern inner Mongolia, China. *J. Geophys. Res. Sol. Earth* **2013**, *118*, 1873–1894. [[CrossRef](#)]
55. Xu, B.; Zhao, P.; Wang, Y.Y.; Liao, W.; Luo, Z.W.; Bao, Q.Z.; Zhou, Y.H. The pre–Devonian tectonic framework of Xing’aneMongolia orogenic belt (XMOB) in North China. *J. Asian Earth Sci.* **2015**, *97*, 183–196. [[CrossRef](#)]
56. Zhu, J.B.; Ren, J.S. Carboniferous–permian stratigraphy and sedimentary environment of Southeastern inner Mongolia, China: Constraints on final closure of the Paleo-Asian Ocean. *Acta Geol. Sin. Engl. Ed.* **2017**, *91*, 832–856. [[CrossRef](#)]
57. Shao, J.A. *Crust Evolution in the Middle Part of the Northern Margin of Sino–Korean Plate*; Beijing University Press: Beijing, China, 1991; pp. 1–138. (In Chinese)
58. Hong, D.W.; Huang, H.Z.; Xiao, Y.J.; Xu, H.M.; Jin, M.Y. Permian alkaline granites in central Inner Mongolia and their geodynamic significance. *Acta Geol. Sin. Engl. Ed.* **1995**, *8*, 27–39.
59. Zhao, C.J.; Peng, Y.J.; Dang, Z.X.; Zhang, Y.P. *Tectonic Framework and Crust Evolution of Eastern Jilin and Heilongjiang Provinces*; Liaoning University Press: Shenyang, China, 1996; pp. 1–186. (In Chinese)
60. Feng, G.Y.; Liu, S.; Zhong, H.; Jia, D.C.; Qi, Y.Q.; Wang, T.; Yang, Y.H. Geochemical characteristics and petrogenesis of late Paleozoic mafic rocks from Yumuchuan, Jilin Province. *Geochimica* **2010**, *39*, 427–438. (In Chinese)
61. Liu, S.; Hu, R.Z.; Gao, S.; Feng, C.X.; Feng, G.Y.; Coulson, I.M.; Li, C.; Wang, T.; Qi, Y.Q. Zircon U–Pb age and Sr–Nd–Hf isotope geochemistry of Permian granodiorite and associated gabbro in the Songliao Block, NE China and implications for growth of juvenile crust. *Lithos* **2010**, *114*, 423–436. [[CrossRef](#)]
62. Chen, B.; Jahn, B.M.; Wilde, S.; Xu, B. Two contrasting Paleozoic magmatic belts in northern Inner Mongolia, China: Petrogenesis and tectonic implications. *Tectonophysics* **2000**, *328*, 157–182. [[CrossRef](#)]
63. Chen, B.; Jahn, B.M.; Tian, W. Evolution of the Solonker suture zone: Constraints from zircon U–Pb ages, Hf isotopic ratios and whole–rock Nd–Sr isotope compositions of subduction– and collision–related magmas and forearc sediments. *J. Asian Earth Sci.* **2009**, *34*, 245–257. [[CrossRef](#)]
64. Jian, P.; Liu, D.Y.; Kröner, A.; Windley, B.F.; Shi, Y.R.; Zhang, W.; Zhang, F.Q.; Miao, L.C.; Zhang, L.Q.; Tomurhuu, D. Evolution of a Permian intraoceanic arc–trench system in the Solonker suture zone, Central Asian Orogenic Belt, China and Mongolia. *Lithos* **2010**, *118*, 169–190. [[CrossRef](#)]
65. Lin, S.Z.; Zhu, G.; Yan, L.J.; Song, L.H.; Liu, B. Structural and chronological constraints on a Late Paleozoic shortening event in the Yanshan Tectonic Belt. *Chin. Sci. Bull.* **2013**, *58*, 3922–3936. [[CrossRef](#)]
66. Wu, F.Y.; Sun, D.Y.; Ge, W.C.; Zhang, Y.B.; Grant, M.L.; Wilde, S.A.; Jahn, B.M. Geochronology of the Phanerozoic granitoids in northeastern China. *J. Asian Earth Sci.* **2011**, *41*, 1–30. [[CrossRef](#)]
67. Zhang, Y.B.; Wu, F.Y.; Wilde, S.A.; Zhai, M.G.; Lu, X.P.; Sun, D.Y. Zircon U–Pb ages and tectonic implications of ‘Early Paleozoic’ granitoids at Yanbian, Jilin Province, northeast China. *Isl. Arc.* **2004**, *13*, 484–505. [[CrossRef](#)]
68. Xu, W.L.; Ji, W.Q.; Pei, F.P.; Meng, E.; Yu, Y.; Yang, D.B.; Zhang, X.Z. Triassic volcanism in eastern Heilongjiang and Jilin provinces, NE China: Chronology, geochemistry, and tectonic implications. *J. Asian Earth Sci.* **2009**, *34*, 392–402. [[CrossRef](#)]
69. Han, J.; Zhou, J.B.; Wang, B.; Cao, J.L. The final collision of the CAOB: Constraint from the zircon U–Pb dating of the Linxi Formation, Inner Mongolia. *Geosci. Front.* **2015**, *6*, 211–225. [[CrossRef](#)]
70. Guo, F.; Li, H.X.; Fan, W.M.; Li, J.Y.; Zhao, L.; Huang, M.W. Variable sediment flux in generation of Permian subduction–related mafic intrusions from the Yanbian region, NE China. *Lithos* **2016**, *261*, 195–215. [[CrossRef](#)]

71. Jia, D.C.; Hu, R.Z.; Lu, Y.; Qiu, X.L. Collision belt between the Khanka block and the north China block in the Yanbian region, Northeast China. *J. Asian Earth Sci.* **2004**, *23*, 211–219.
72. Wang, F.; Xu, W.L.; Xu, Y.G.; Gao, F.H.; Ge, W.C. Late Triassic bimodal igneous rocks in eastern Heilongjiang Province, NE China: Implications for the initiation of subduction of the Paleo–Pacific Plate beneath Eurasia. *J. Asian Earth Sci.* **2015**, *97*, 406–423. [[CrossRef](#)]
73. Zhou, J.P.; Liu, Y.J.; Li, W.M.; Wen, Q.B.; Liang, C.Y.; Feng, Z.Q. Eastern extension of the Solonker-Xar Moron-Changchun-Yanji Suture Zone: Constraints from thermochronology of sedimentary and mafic rocks in the Hunchun-Yanji area, Northeast China. *Geol. J.* **2019**, *54*, 679–697. [[CrossRef](#)]
74. Han, Y.G.; Zhao, G.C. Final amalgamation of the Tianshan and Junggar orogenic collage in the southwestern Central Asian Orogenic Belt: Constraints on the closure of the Paleo-Asian Ocean. *Earth-Sci. Rev.* **2018**, *186*, 129–152. [[CrossRef](#)]
75. Hou, Q.L.; Guo, Q.Q.; Fang, A.M. Discussions on some basic problems in the research of orogenic belts concerning on flysch and molasse. *Acta Petrol. Sin.* **2018**, *34*, 1885–1896. (In Chinese)
76. Hsiung, K.H.; Yu, H.S.; Su, M. Sedimentation in remnant ocean basin off SW Taiwan with implication for closing northeastern South China Sea. *J. Geol. Soc.* **2015**, *172*, 641–647. [[CrossRef](#)]
77. Fan, J.J.; Li, C.; Wang, M.; Xie, C.M. Reconstructing in space and time the closure of the middle and western segments of the BangongNujiang Tethyan Ocean in the Tibetan Plateau. *Int. J. Earth Sci.* **2018**, *107*, 231–249. [[CrossRef](#)]
78. Su, Y.Z. The strata of Permian period and Early Triassic period in the Northeast of China. *Jilin Geol.* **1996**, *15*, 55–65.
79. Su, Y.Z. The Paleozoic Era stratum in Songhua River stratum area. *Jilin Geol.* **1996**, *15*, 35–39.
80. JBGMR (Jilin Bureau of Geology and Mineral Resources). *Regional Geology of Jilin Province*; Geological Publishing House: Beijing, China, 1988; pp. 1–698. (In Chinese)
81. Whitney, D.L.; Evans, B.W. Abbreviations for names of rock-forming minerals. *Am. Mineral.* **2010**, *95*, 185–187. [[CrossRef](#)]
82. Hoskin, P.W.O.; Schaltegger, U. The Composition of Zircon and Igneous and Metamorphic Petrogenesis. *Rev. Mineral. Geochem.* **2003**, *53*, 27–62. [[CrossRef](#)]
83. Jiang, Z.W.; Luo, J.L.; Liu, X.S.; Hu, X.Y.; Ma, S.W.; Hou, Y.D.; Fan, Y.L.; Hu, Y.H. Provenance and Implication of Carboniferous–Permian Detrital Zircons from the Upper Paleozoic, Southern Ordos Basin, China: Evidence from U–Pb Geochronology and Hf Isotopes. *Minerals* **2020**, *10*, 265. [[CrossRef](#)]
84. Cao, Y.T.; Liu, L.; Chen, D.L.; Wang, C.; Yang, W.Q.; Kang, L.; Zhu, X.H. Partial melting during exhumation of Paleozoic retrograde eclogite in North Qaidam, western China. *J. Asian Earth Sci.* **2017**, *148*, 223–240. [[CrossRef](#)]
85. Cao, Y.T.; Liu, L.; Wang, C.; Kang, L.; Li, D.; Yang, W.Q.; Zhu, X.H. Timing and nature of the partial melting processes during the exhumation of the garnet-bearing biotite gneiss in the southern Altyn Tagh HP/UHP belt, Western China. *J. Asian Earth Sci.* **2019**, *170*, 274–293. [[CrossRef](#)]
86. Wang, S.J.; Li, X.P.; Schertl, H.P.; Feng, Q.D. Petrogenesis of early cretaceous andesite dykes in the Sulu orogenic belt, eastern China. *Miner. Petrol.* **2019**, *113*, 77–97. [[CrossRef](#)]
87. Yang, J.H.; Wu, F.Y.; Shao, J.A.; Wilde, S.A.; Xie, L.W.; Liu, X.M. Constraints on the timing of uplift of the Yanshan Fold and Thrust Belt, North China. *Earth Planet. Sci. Lett.* **2006**, *246*, 336–352. [[CrossRef](#)]
88. Peccerillo, A.; Taylor, A.R. Geochemistry of Eocene calc-alkaline volcanic rocks from the Kastamonu area, Northern Turkey. *Contrib. Mineral. Petrol.* **1976**, *58*, 63–81. [[CrossRef](#)]
89. Middlemost, E.A. Naming materials in the magma/igneous rock system. *Earth-Sci. Rev.* **1994**, *37*, 215–224. [[CrossRef](#)]
90. Maniar, P.D.; Piccoli, P.M. 1989. Tectonic discrimination of granitoids. *Geol. Soc. Am. Bull.* **1989**, *101*, 635–643. [[CrossRef](#)]
91. Sun, S.S.; McDonough, W.F. Chemical and isotopic systematics of oceanic basalts: Implications for mantle composition and processes. In *Magmatism in Ocean Basins*; Saunders, A.D., Norry, M.J., Eds.; Geological Society of London Special Publication: London, UK, 1989; Volume 42, pp. 313–345.
92. Du, L.; Long, X.P.; Yuan, C.; Zhang, Y.Y.; Huang, Z.Y.; Sun, M.; Zhao, G.C.; Xiao, W.J. Early Paleozoic Dioritic and Granitic Plutons in the Eastern Tianshan Orogenic Belt, NW China: Constraints on the Initiation of a Magmatic Arc in the Southern Central Asian Orogenic Belt. *J. Asian Earth Sci.* **2018**, *153*, 139–153. [[CrossRef](#)]
93. Du, L.; Long, X.P.; Yuan, C.; Zhang, Y.Y.; Huang, Z.Y.; Wang, X.Y.; Yang, Y.H. Mantle contribution and tectonic transition in the Aqishan-Yamansu Belt, Eastern Tianshan, NW China: Insights from geochronology and geochemistry of Early Carboniferous to Early Permian felsic intrusions. *Lithos* **2018**, *304–307*, 230–244. [[CrossRef](#)]
94. Du, L.; Long, X.P.; Yuan, C.; Zhang, Y.Y.; Huang, Z.Y.; Sun, M.; Xiao, W.J. Petrogenesis of late paleozoic diorites and a-type granites in the central Eastern Tianshan, NW China: Response to post-collisional extension triggered by slab breakoff. *Lithos* **2018**, *318–319*, 47–59. [[CrossRef](#)]
95. Meng, Y.K.; Xiong, F.H.; Xu, Z.Q.; Ma, X.X. Petrogenesis of Late Cretaceous mafic enclaves and their host granites in the Nyemo region of southern Tibet: Implications for the tectonic-magmatic evolution of the Central Gangdese Belt. *J. Asian Earth Sci.* **2019**, *176*, 27–41. [[CrossRef](#)]
96. Du, L.; Zhang, Y.Y.; Huang, Z.Y.; Li, X.P.; Yuan, C.; Wu, B.; Long, X.P. Devonian to carboniferous tectonic evolution of the Kangguer Ocean in the Eastern Tianshan, NW China: Insights from three episodes of granitoids. *Lithos* **2019**, *350–351*, 105243. [[CrossRef](#)]
97. Du, L.; Yuan, C.; Li, X.P.; Zhang, Y.Y.; Huang, Z.Y.; Long, X.P. Petrogenesis and Geodynamic Implications of the Carboniferous Granitoids in the Dananhu Belt, Eastern Tianshan Orogenic Belt. *J. Earth Sci.* **2019**, *30*, 1243–1252. [[CrossRef](#)]

98. Gehrels, G. Detrital Zircon U-Pb geochronology applied to tectonics. *Annu. Rev. Earth Planet. Sci.* **2014**, *42*, 127–149. [[CrossRef](#)]
99. Chappell, B.W. Aluminium saturation in I- and S-type granites and the characterization of fractionated haplogranites. *Lithos* **1999**, *46*, 535–551. [[CrossRef](#)]
100. Chappell, B.W.; White, A.J.R. Two contrasting granite types. *Pac. Geol.* **1974**, *8*, 173–174.
101. Chappell, B.W.; White, A.J.R. I- and S-type granites in the Lachlan Fold Belt. *Earth Environ. Sci. Trans. R. Soc. Edinb.* **1992**, *83*, 1–26.
102. Chappell, B.W.; White, A.J.R. Two contrasting granite types: 25 years later. *Aust. J. Earth Sci.* **2001**, *48*, 489–499. [[CrossRef](#)]
103. Whalen, J.B.; Currie, K.L.; Chappell, B.W. A-type granites: Geochemical characteristics, discrimination and petrogenesis. *Contrib. Mineral. Petrol.* **1987**, *95*, 407–419. [[CrossRef](#)]
104. King, P.L.; White, A.J.R.; Chappell, B.W. Characterization and origin of aluminous A-type granites from the Lachlan Fold Belt, southeastern Australia. *J. Petrol.* **1997**, *38*, 371–391. [[CrossRef](#)]
105. Watson, E.B.; Harrison, T.M. Zircon saturation revisited: Temperature and composition effects in a variety of crustal magma types. *Earth Planet. Sci. Lett.* **1983**, *64*, 295–304. [[CrossRef](#)]
106. Miller, C.F.; McDowell, S.M.; Mapes, R.W. Hot and cold granites? Implications of zircon saturation temperatures and preservation of inheritance. *Geology* **2003**, *31*, 529–532. [[CrossRef](#)]
107. Boehnke, P.; Watson, E.B.; Trail, D.; Harrison, M.; Schmitt, A.K. Zircon saturation re-revisited. *Chem. Geol.* **2013**, *351*, 324–334. [[CrossRef](#)]
108. Martin, H.; Smithies, R.H.; Moyen, J.F.; Champion, D. An overview of adakite, tonalite–trondhjemite–granodiorite (TTG), and sanukitoid: Relationships and some implications for crustal evolution. *Lithos* **2013**, *79*, 1–24. [[CrossRef](#)]
109. Rollinson, H.R. *Using Geochemical Data: Evaluation, Presentation, Interpretation*; Pearson Education Limited: London, UK, 1993; pp. 108–111.
110. Fedo, C.M.; Sircombe, K.N.; Rainbird, R.H. Detrital zircon analysis of the sedimentary record. *Rev. Mineral. Geochem.* **2003**, *53*, 277–303. [[CrossRef](#)]
111. Böhm, C.O.; Heaman, L.M.; Creaser, R.A.; Corkery, M.T. Discovery of pre-3.5 Ga exotic crust at the northwestern Superior Province margin, Manitoba. *Geology* **2000**, *28*, 75–78. [[CrossRef](#)]
112. Cawood, P.A.; Nemchin, A.A. Provenance record of a rift basin: U/Pb ages of detrital zircons from the Perth Basin, Western Australia. *Sediment. Geol.* **2000**, *134*, 209–234. [[CrossRef](#)]
113. Zhang, S.H.; Zhao, Y.; Yang, Z.Y.; He, Z.F.; Wu, H. The 1.35Ga diabase sills from the northern North China Craton: Implications for breakup of the Columbia (Nuna) supercontinent. *Earth Planet. Sci. Lett.* **2009**, *288*, 588–600. [[CrossRef](#)]
114. Zhang, S.H.; Zhao, Y.; Ye, H.; Liu, J.M.; Hu, Z.C. Origin and evolution of the Bainaimiao arc belt: Implications for crustal growth in the southern Central Asian orogenic belt. *Geol. Soc. Am. Bull.* **2014**, *126*, 1275–1300. [[CrossRef](#)]
115. Meng, E.; Xu, W.L.; Pei, F.P.; Yang, D.B.; Yu, Y.; Zhang, X.Z. Detrital-zircon geochronology of late paleozoic sedimentary rocks in Eastern Heilongjiang Province, NE China: Implications for the tectonic evolution of the Eastern segment of the Central Asian orogenic belt. *Tectonophysics* **2010**, *485*, 42–51. [[CrossRef](#)]
116. Yang, H.; Ge, W.C.; Zhao, G.C.; Yu, J.J.; Zhang, Y.L. Early Permian-Late Triassic granitic magmatism in the Jiamusi-Khanka Massif, eastern segment of the Central Asian Orogenic Belt and its implications. *Gondwana Res.* **2015**, *27*, 1509–1533. [[CrossRef](#)]
117. Ma, H.T.; Ma, X.; Chen, J.F.; Chen, B.; Li, C.; Zhou, L.M.; Yang, H.Z. The Zhangjiatun igneous complex in the southeastern margin of the Central Asian Orogenic Belt, NE China: Evidence for an Early Paleozoic intra-oceanic arc. *J. Asian Earth Sci.* **2020**, *194*, 104182. [[CrossRef](#)]
118. Pei, F.P.; Zhang, Y.; Wang, Z.W.; Cao, H.H.; Xu, W.L.; Wang, F.; Yang, C. Early-Middle Paleozoic subduction–collision history of the south-eastern Central Asian Orogenic Belt: Evidence from igneous and metasedimentary rocks of central Jilin Province, NE China. *Lithos* **2016**, *261*, 164–180. [[CrossRef](#)]
119. Grove, T.L.; Elkins-Tanton, L.T.; Parman, S.W.; Chatterjee, N.; Müntener, O.; Gaetani, G.A. Fractional crystallization and mantle-melting controls on calc-alkaline differentiation trends. *Contrib. Mineral. Petrol.* **2003**, *145*, 515–533. [[CrossRef](#)]
120. Pearce, J.A.; Harris, N.B.W.; Tindle, A.G. Trace element discrimination diagrams for the tectonic interpretation of granitic rocks. *J. Petrol.* **1984**, *25*, 956–983. [[CrossRef](#)]
121. Defant, M.J.; Drummond, M.S. Derivation of some modern arc magmas by melting of young subducted lithosphere. *Nature* **1990**, *347*, 662–665. [[CrossRef](#)]
122. Martin, H. Effect of steeper Archaean geothermal gradient on geochemistry of subduction-zone magmas. *Geology* **1986**, *14*, 753–756. [[CrossRef](#)]
123. Yuan, H.L.; Gao, S.; Liu, X.M.; Li, H.M.; Günther, D.; Wu, F.Z. Accurate U–Pb age and trace element determinations of zircon by laser ablation inductively coupled plasma mass spectrometry. *Geostand. Geoanal. Res.* **2004**, *28*, 353–370. [[CrossRef](#)]
124. Van Achterbergh, E.; Ryan, C.G.; Jackson, S.E.; Griffin, W.L. Data reduction software for LA-ICP-MS. In *Laser-ablation-ICP-MS Spectrometry in the Earth Sciences: Principles and Applications*; Sylvester, P.J., Ed.; Mineralogical Association of Canada, MAC Short Course Series: Ottawa, ON, Canada, 2001; pp. 239–243.
125. Ludwig, K.R. *User's Manual for Isoplot 3.00: A Geochronological Toolkit for Microsoft Excel*; Berkeley Geochronology Center: Berkeley, CA, USA, 2003; Volume 4, pp. 1–70.
126. Yuan, H.L.; Gao, S.; Dai, M.N.; Zong, C.L.; Günther, D.; Fontaine, G.H.; Liu, X.M.; Diwu, C.R. Simultaneous determinations of U–Pb age, Hf isotopes and trace element compositions of zircon by excimer laser-ablation quadrupole and multiple-collector ICP-MS. *Chem. Geol.* **2008**, *247*, 100–118. [[CrossRef](#)]

-
127. Rudnick, R.L.; Gao, S.; Ling, W.L.; Liu, Y.S.; McDonough, W.F. Petrology and geochemistry of spinel peridotite xenoliths from Hannuoba and Qixia, North China craton. *Lithos* **2004**, *7*, 609–637. [[CrossRef](#)]
 128. Li, X.H.; Liu, D.Y.; Sun, M.; Li, W.X.; Liang, X.R.; Liu, Y. Precise Sm-Nd and U-Pb isotopic dating of the super-giant Shizhuyuan polymetallic deposit and its host granite, Southeast China. *Geol. Mag.* **2004**, *141*, 225–231. [[CrossRef](#)]